Chapter 10

Fractional Quantum Hall States of Bosons: Properties and Prospects for Experimental Realization

N. R. Cooper

*T.C.M. Group, Cavendish Laboratory, J.J. Thomson Avenue,
University of Cambridge, Cambridge CB3 0HE, United Kingdom
nrc25@cam.ac.uk*

An overview is given of experimental settings in which one can expect to observe fractional quantum Hall states of bosons. The focus is placed on ultracold atomic gases, and the regimes most likely to allow the realization of fractional quantum Hall states. The means by which Landau levels, or other topological energy bands, can be generated for cold atoms are summarized. The current theoretical understanding of the likely many-body phases is then presented, focusing on the models that are most readily studied experimentally. The chapter concludes by making contact with other physical platforms where bosonic fractional quantum Hall states are expected to appear: in quantum magnets, engineered qubit arrays and polariton systems.

Contents

1. Introduction

To date all experimental realizations of fractional quantum Hall (FQH) states have been for electrons. The FQH effect was first discovered in modulated-doped gallium arsenide quantum wells,[1] and much of the subsequent exploration of these states has been in similar devices. More recently, studies have progressed to graphene structures, where new features arise, e.g. in superlattice structures.[2]

Despite the experimental prevalence of fermionic FQH states, the theory of the FQH effect can be readily applied to interacting bosonic particles. Notably, the Laughlin wave function[3] describes a FQH state of bosons at filling factor $\nu = 1/p$ when p is an even integer. Similarly, all other model wave functions of fractional quantum Hall states can be converted between fermionic and bosonic variants. It is natural to ask where bosonic FQH states might be found in nature.

In an insightful early contribution, Kalmeyer and Laughlin proposed that the Laughlin state of bosons might describe the ground state of the spin-1/2 Heisenberg antiferromagnet on a triangular lattice.[4] Although subsequent work has shown this not to be the case for that model, the Laughlin state of bosons is believed to describe the ground state of quantum magnets on other frustrated lattices. The relevance of the Laughlin state, and other FQH states, for quantum magnets and related systems will be discussed further below.

The development of the field of ultracold atomic gases has allowed the exploration of quantum many body phases of bosonic and fermionic atoms in a variety of novel settings.[5] These hold the promise of realizing FQH states for both bosonic and fermionic species. In typical settings the bosonic species are more easily cooled to regimes of quantum degeneracy, so the pursuit of bosonic FQH states is a natural goal. Theoretical work has established the conditions under which bosonic FQH states could arise for cold gases of bosons, as well as the forms of these states, in a variety of experimental settings under active investigation. While FQH states take the same qualitative forms for bosons as for fermions, determining the nature of the many body ground state is a delicate issue that depends on a fine balance of energetics related to the specific physical realization. Thus, it is important to study the bosonic models theoretically to assess which, if any, FQH states are stable in realistic physical settings. One notable finding that we highlight below is that the experimentally relevant models for interacting bosons have non-Abelian phases that are more stable than their fermionic counterparts in typical electronic systems.

In Sec. 2 we give an overview of prospects of achieving FQH states for ultracold atomic gases. We focus on bosonic particles, but comment also on fermionic atomic gases in situations for which the cold gas realizations have qualitative differences from conventional electronic systems. For bosonic realizations, we describe theoretical results indicating possible stability of non-Abelian fractional quantum Hall phases, and also for unconventional FQH states on lattices. We conclude in Sec. 3 by describing possibilities for the achievement of FQH states of bosons in other physical settings: in quantum spin systems, synthetic quantum spin systems and photonic materials.

2. Ultracold Atomic Gases

The development of techniques to trap and to cool gases of neutral atoms have made it a routine matter to bring dilute atomic gases into regimes of quantum degeneracy.[5] Although these cold dilute gases exist only as metastable states, the true equilibrium phases being dense crystals, the lifetimes to collapse are very long as a result of the very low densities used, $n_{3D} \sim 10^{14} \text{cm}^{-3}$, which make the three-body collisions required for collapse very rare. Such low densities imply correspondingly low temperatures for the so-called "ultracold" regime of quantum degeneracy. For the thermal de Broglie wavelength, $\lambda_T \sim \hbar/\sqrt{Mk_B T}$ (for atoms of mass M) to be larger than the inter-particle spacing, $n_{3D}^{-1/3}$, requires cooling to below micro-Kelvin temperatures for typical atomic species.

Under these ultracold conditions the thermal wavelength λ_T is also much larger than the range of the inter-particle interaction, so the collisional properties are accurately described by the s-wave scattering length a_s. The s-wave scattering may then be represented by a pairwise contact repulsion $V(\boldsymbol{r}) = g_{3D}\delta^3(\boldsymbol{r})$ with $g_{3D} = 4\pi\hbar^2 a_s/M$, and suitable regularization.[5] For weakly interacting bosons, which form a Bose–Einstein condensate at low temperatures, the strength of interactions is conveniently expressed in terms of the chemical potential $\mu = g_{3D}n_{3D}$.[6]

Throughout this chapter we shall be concerned with quasi-two-dimensional geometries, in which the atoms are restricted to the xy-plane by a tight harmonic confinement in the z-direction. When the energy spacing of the sub-bands of the z confinement, $\hbar\omega_z$, is large compared to the chemical potential, μ, the atoms can be approximated as occupying the lowest sub-band. The effective 2D interaction becomes $V(\boldsymbol{r}) = g_{2D}\delta^2(\boldsymbol{r})$ with $g_{2D} = g_{3D}/(\sqrt{2\pi}a_z)$ and $a_z = \sqrt{\hbar^2/M\omega_z}$. The strength of the interaction between atoms can be widely varied by tuning close to a scattering resonance: either a Feshbach resonance[5] (involving a weakly bound state of the two atoms); or a confinement-induced resonance[7] (involving coupling to transverse sub-band modes). The functional form of the interaction can also be changed, notably by use of atoms (or molecules) with large magnetic (or electric) dipole moments which allow interactions that fall as $1/r^3$ and that can be spatially anisotropic.[8]

2.1. *Landau levels and Chern bands*

In order to search for FQH states of bosonic atoms, stabilized by their inter-particle interactions, one first needs to find ways by which one can form Landau levels — or other suitable flat-band energy spectra — for the individual atoms. To generate Landau levels, one must confront the question of how to cause *neutral* atoms to experience the orbital effects that a uniform magnetic field has on a charged particle. This can be achieved in a variety of ways. We outline some of them here, restricting discussions to the essential physics needed in order to understand the forms of the relevant microscopic models. More comprehensive reviews exist for rotating gases[9,10] and for topological optical lattices.[11]

2.1.1. *Rotation*

An intuitively simple means by which to impose an effective magnetic field on a gas of neutral atoms is to put the gas into rotation. In a frame of reference rotating at angular frequency $\boldsymbol{\Omega}$ an atom of mass M moving at velocity $\boldsymbol{v}$ experiences a Coriolis force $2M\boldsymbol{v} \times \boldsymbol{\Omega}$. This has the same form as a Lorentz force $q\boldsymbol{v} \times \boldsymbol{B}$ on a charge q in magnetic field $\boldsymbol{B}$, provided one makes the association

$$q\boldsymbol{B} = 2M\boldsymbol{\Omega}\,. \tag{1}$$

This simple classical observation can be made precise, also in its extension to the quantum description, by noting that the transformation to the rotating frame acts to convert the Hamiltonian in the laboratory frame H_0 to

$$H_\Omega = H_0 - \boldsymbol{\Omega} \cdot \boldsymbol{L}\,, \tag{2}$$

where $\boldsymbol{L} = \boldsymbol{r} \times \boldsymbol{p}$ is the angular momentum operator.[12] For a particle in an isotropic 2D harmonic trap of natural frequency ω_0, the Hamiltonian in a frame rotating at angular velocity $\boldsymbol{\Omega} = \Omega\boldsymbol{e}_z$ is then

$$H_\Omega = \frac{\boldsymbol{p}^2}{2M} + \frac{1}{2}M\omega_0^2\boldsymbol{r}^2 - \boldsymbol{\Omega} \cdot \boldsymbol{r} \times \boldsymbol{p}\,. \tag{3}$$

This may be rewritten

$$H_\Omega = \frac{(\boldsymbol{p} - M\boldsymbol{\Omega} \times \boldsymbol{r})^2}{2M} + \frac{1}{2}M(\omega_0^2 - \Omega^2)\boldsymbol{r}^2\,, \tag{4}$$

showing that it can be viewed as describing a 2D particle of charge q coupled to a vector potential via $q\boldsymbol{A} = M\boldsymbol{\Omega} \times \boldsymbol{r}$. Taking the curl recovers Eq. (1), and gives a flux density

$$n_\phi \equiv \frac{qB}{h} = \frac{2M\Omega}{h}\,. \tag{5}$$

The harmonic confinement in Eq. (4) is reduced by the centrifugal force, and vanishes at $\Omega = \omega_0$. At this special value, the Hamiltonian describes a free particle in a uniform magnetic field, with cyclotron energy $\hbar\omega_c = 2\hbar\Omega = 2\hbar\omega_0$ and the effective magnetic length $\ell_B = \sqrt{\hbar/qB} = \sqrt{\hbar/2M\omega_0}$. The lowest energy states are the usual lowest Landau level wavefunctions

$$\phi_m(z) \propto z^m \exp(-|z|^2/4)\,, \tag{6}$$

where $z = (x + \mathrm{i}y)/\ell_B$, and $m = 0, 1, 2, \ldots$.

Although these wavefunctions have been derived for the fine-tuned case $\Omega = \omega_0$, in fact they are exact energy eigenstates for any rotation rate Ω. This can be understood by noting that the effect of the rotation, Eq. (2), is simply to shift the energies of the 2D harmonic oscillator by an amount that depends on the angular momentum about the z-axis. Since this component of angular momentum is conserved, the energy eigenstates are unaffected by the rotation, Ω. Writing the energy of the 2D oscillator in terms of the radial quantum number $n_r = 0, 1, 2, \ldots$ and angular momentum $m = \ldots, -2, -1, 0, 1, 2, \ldots$, the spectrum is[13]

$$E_\Omega = \hbar\omega_0(2n_r + |m| + 1) - m\hbar\Omega\,. \tag{7}$$

This spectrum is plotted in Fig. 1 for $\Omega = 0$ and $\Omega = \omega_0$. The special point $\Omega = \omega_0$ recovers the Landau level spectrum, Fig. 1(b). For $\Omega < \omega_0$ the Landau level wavefunctions remain the same, but are shifted in energy by a residual harmonic confinement, leading to the m-dependent term $\hbar(\omega_0 - \Omega)m$ for the orbitals in the lowest Landau level, for which $m > 0$.
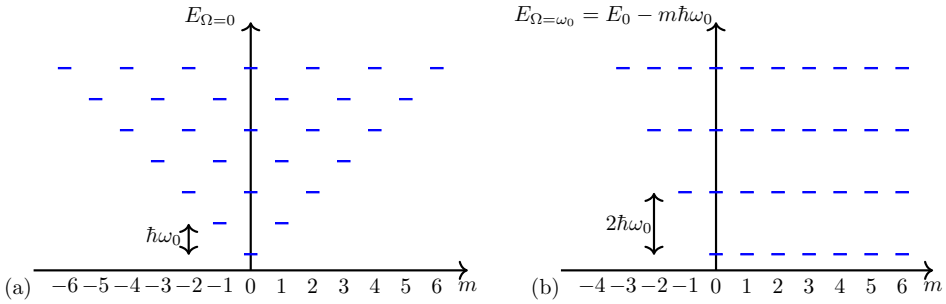

Fig. 1.   (a) Spectrum of the isotropic 2D harmonic oscillator, Eq. (7), of natural frequency ω_0 as a function of angular momentum quantum number m. (b) In a frame rotating at angular frequency Ω, the spectrum is $E_\Omega = E_0 - \Omega\hbar m$. For $\Omega = \omega_0$ the spectrum, $E_{\omega_0} = E_0 - m\hbar\omega_0$, is the Landau level spectrum of a charged particle in a uniform magnetic field, with cyclotron energy $2\hbar\omega_0$.

Experiments on atomic Bose–Einstein condensates put into rotation by mechanical stirring have allowed studies of quantum degenerate bosons in regimes in which the chemical potential μ is less than both the sub-band spacing $\hbar\omega_z$ and the cyclotron energy $\hbar\omega_c = 2\hbar\Omega$, that is in the 2D lowest Landau level regime.[14] That said, these studies have so far been restricted to regimes of high particle density where the gases show vortex lattices. The conditions under which FQH states can appear, and the nature of these states, will be discussed in detail below. For now, note that the limitation $\Omega \leq \omega_0$ restricts the flux density (5) to $n_\phi \leq 2M\omega_0/h$. In turn, for a fractional quantum Hall state with 2D particle density $n_{2D} \sim n_\phi$, the interaction energy is of order $\mu \sim g_{2D}n_\phi$, so is restricted to $\mu \lesssim g_{2D}(2M\omega_0/h) \sim \hbar\omega_0(a_s/a_z)$. Typical magnetic traps have a frequency scale $\omega_0 = 2\pi \times (10 - 100)$Hz, and a_s/a_z is a small number, giving an interaction scale μ below the *pico*-Kelvin energy scale. This is an extremely small temperature, much smaller than the temperatures to which it is currently possible to cool atomic gases. The situation can be improved by using for atoms with large a_s (e.g. resonant interactions), or by using very tight traps to increase ω_0, as in Ref. 15 or in quantum gas microscopes.[16]

2.1.2. *Optically dressed states*

The limitation of small flux densities achievable by rotation in typical atomic gases has motivated the development of other ways to generate artificial magnetic fields for cold atoms. One very powerful way to accomplish this, which plays to the strengths of atomic gases, is through optically dressed states.[17]

Optical dressing refers to the use of coherent optical fields to place the atom into a well-defined superposition of internal levels, through the control of the amplitudes and phases of light fields that couple these levels. For a two-level system, coherent driving at frequency ω leads to the coupling

$$\hat{V}(t) = \begin{pmatrix} \epsilon_1 & \Omega\cos(\omega t - \phi) \\ \Omega\cos(\omega t - \phi) & \epsilon_2 \end{pmatrix},\tag{8}$$

with the matrix expressed in the basis formed by the two internal energy levels. (We use hats to denote operators acting within the space of internal energy levels.) Through a suitable time-dependent gauge transformation one can replace $\cos(\omega t - \phi)$ by $(1/2)[\exp(-i\phi) + \exp(-2i\omega t + i\phi)]$. Then, provided ω is large compared to all other relevant frequency scales, one can make the rotating wave approximation (RWA)[17] by which the remaining oscillating term vanishes, to give a time-independent coupling

$$\hat{V}_{\mathrm{RWA}} = \frac{\epsilon_1 + \epsilon_2}{2}\hat{1} + \frac{\Delta}{2}\hat{\sigma}_z + \frac{\Omega}{2}(\cos\phi\hat{\sigma}_x + \sin\phi\hat{\sigma}_y),\tag{9}$$

where $\Delta = \epsilon_1 - \epsilon_2 - \hbar\omega$ and $\hat{\sigma}_i$ are the conventional Pauli matrices. Of course, for this simple situation, the phase ϕ could also be removed by a gauge transformation. However, we leave it to emphasize the greater generality of the form of optical coupling: we will be interested in settings where the optical fields lead to *spatially varying* parameters Ω, Δ and ϕ for which one cannot, in general, choose a gauge in which ϕ vanishes everywhere.

The optically dressed states are the eigenstates of this RWA coupling (9). Although presented for a two-level system, these considerations can apply more generally for N_I coupled internal states. Consider an atom localized in space at a position $\boldsymbol{r}$, and subjected to local optical fields at this point that couple these N_I levels. We denote the dressed states at this location by $|n_{\boldsymbol{r}}\rangle$ with energies $E_n(\boldsymbol{r})$, with $n = 1 \ldots N_\mathrm{I}$. We use these states as a local basis for a general atomic state

$$|\psi(\boldsymbol{r})\rangle = \sum_n \psi_n(\boldsymbol{r})|n_{\boldsymbol{r}}\rangle.\tag{10}$$

Including the kinetic energy of the atom leads to the full Hamiltonian

$$\hat{H} = \sum_n \left[\frac{\boldsymbol{p}^2}{2M} + E_n(\boldsymbol{r})\right]|n_{\boldsymbol{r}}\rangle\langle n_{\boldsymbol{r}}|.\tag{11}$$

Provided the motion of the particle is slow, in the sense that the typical kinetic energy $\langle \boldsymbol{p}^2\rangle/2M$ is small compared to the energy spacings $E_{n+1} - E_n$, then to a good approximation one can project the Hamiltonian onto states labeled by n alone (ignoring mixing between different dressed states). The effective Hamiltonian for this adiabatic evolution of the nth state, obtained from $H_n\psi_n = \langle n_{\boldsymbol{r}}|H\psi_n|n_{\boldsymbol{r}}\rangle$, is

$$H_n = \frac{(\boldsymbol{p} - q\boldsymbol{A})^2}{2M} + V_n(\boldsymbol{r}),\tag{12}$$

where

$$qA = i\hbar\langle n_{\boldsymbol{r}}|\boldsymbol{\nabla}n_{\boldsymbol{r}}\rangle\,, \tag{13}$$

$$V_n(\boldsymbol{r}) = E_n(\boldsymbol{r}) + \frac{\hbar^2}{2M}\left(\langle\boldsymbol{\nabla}n_{\boldsymbol{r}}|\boldsymbol{\nabla}n_{\boldsymbol{r}}\rangle - |\langle n_{\boldsymbol{r}}|\boldsymbol{\nabla}n_{\boldsymbol{r}}\rangle|^2\right)\,. \tag{14}$$

Note the appearance of a gauge field (13): the Berry connection arising from the (spatial) parallel transport of the local state $|n_{\boldsymbol{r}}\rangle$. The associated Berry phase accumulated as the atom moves in the xy-plane plays the role of the Aharonov–Bohm phase of a charged particle moving in an effective magnetic field. The effective Berry curvature in real space determines the flux density experienced by the particle. This approach was implemented in pioneering experiments reported in Ref. 18, which used three internal states of rubidium-87 to generate an effective magnetic field acting on a Bose–Einstein condensate. The scheme used in this experiment gives a vector potential of order $qA \lesssim \hbar/\lambda$, with λ the optical wavelength. Consequently, the total flux through a region of linear size R is limited to $N_\phi \lesssim \hbar R/\lambda$, and the flux density is limited to $n_\phi \lesssim 1/(R\lambda)$ which is small for typical systems $R \gg \lambda$.

The flux densities achievable using optically dressed states can be vastly increased by forming *optical flux lattices*,[19] in which the optical fields have vortices. The associated phase singularities cause qA to exceed $\hbar/\lambda$, effectively forming Dirac strings, and allowing a magnetic flux density of order $n_\phi \sim N_{\rm I}/\lambda^2$. An example of an optical flux lattice for a two-state system is given by

$$\hat{V}_{\rm RWA}(\boldsymbol{r}) = \mathcal{V}_0\begin{pmatrix} \cos[\boldsymbol{r}\cdot(\boldsymbol{\kappa}_1+\boldsymbol{\kappa}_2)] & \cos(\boldsymbol{r}\cdot\boldsymbol{\kappa}_1) - i\cos(\boldsymbol{r}\cdot\boldsymbol{\kappa}_2) \\ \cos(\boldsymbol{r}\cdot\boldsymbol{\kappa}_1) + i\cos(\boldsymbol{r}\cdot\boldsymbol{\kappa}_2) & -\cos[\boldsymbol{r}\cdot(\boldsymbol{\kappa}_1+\boldsymbol{\kappa}_2)] \end{pmatrix}\,, \tag{15}$$

where $\boldsymbol{\kappa}_{1,2}$ are the two basis vectors of the lattice. Figure 2(c) shows the resulting local flux density for the case where $\boldsymbol{\kappa}_{1,2}$ are of equal length and at 120-degrees to each other, giving a lattice with triangular symmetry.

The local flux density is non-uniform but has a nonzero average. One thus expects the low energy states to mimic those of the continuum Landau level. In this lattice setting, the appropriate way to characterize these 2D energy bands is in terms of their Chern numbers.[20] Indeed, the lowest band of the above optical flux lattice (15) is readily shown to have a Chern number of unit magnitude, $|\mathcal{C}| = 1$, consistent with that of the lowest Landau level. (This result holds true for any finite value of the ratio $\mathcal{V}_0/E_R$ of the lattice depth, $\mathcal{V}_0$, to the recoil energy, $E_R = \hbar^2\kappa^2/2M$, which sets the characteristic kinetic energy.)

The most complete understanding of optical flux lattices is achieved by considering the action of the optical fields in reciprocal space.[21] In essence the optical flux lattice involves a series of momentum exchanges $\boldsymbol{\kappa}_i$ with amplitude and phase defined by the matrix elements $V_{\boldsymbol{\kappa}}^{\alpha'\alpha} = \langle\alpha', \boldsymbol{q}+\boldsymbol{\kappa}|\hat{V}_{\rm RWA}|\alpha, \boldsymbol{q}\rangle$. Here $\alpha, \alpha' = 1, \ldots, N_{\rm I}$ label the undressed internal states. If the optical fields are to define a periodic lattice (as opposed to a quasi-crystal), this set of couplings must form a regular lattice in reciprocal space. For example, Fig. 3(a) shows a generalization of the
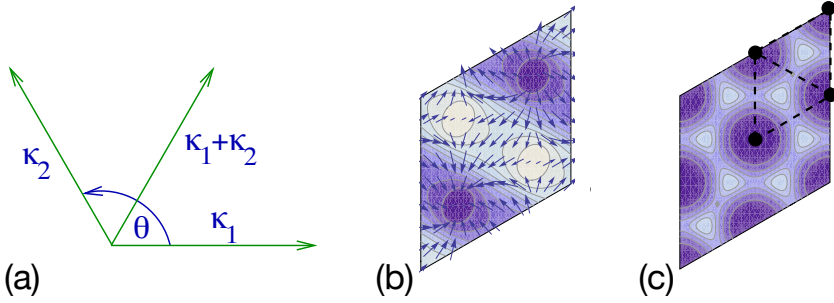
Fig. 2. Illustration of the optical flux lattice formed by coupling two internal atomic levels in the manner of Eq. (15). (a) The momentum transfers $\boldsymbol{\kappa}_{1,2}$ are depicted at an angle of $\theta = 2\pi/3$. (b) The spatial variation of the lowest energy dressed state $n_{\boldsymbol{r}}$ in the real space unit cell is illustrated: arrows denote the two components $\langle n_{\boldsymbol{r}}|\hat{\sigma}_{x,y}|n_{\boldsymbol{r}}\rangle$; contours and shading denote $\langle n_{\boldsymbol{r}}|\hat{\sigma}_z|n_{\boldsymbol{r}}\rangle$. These variations lead to non-trivial Berry connection in real space (13). The local flux density, given by the curl of the real space Berry connection, is spatially varying but with nonzero average. Adapted from Ref. 19.
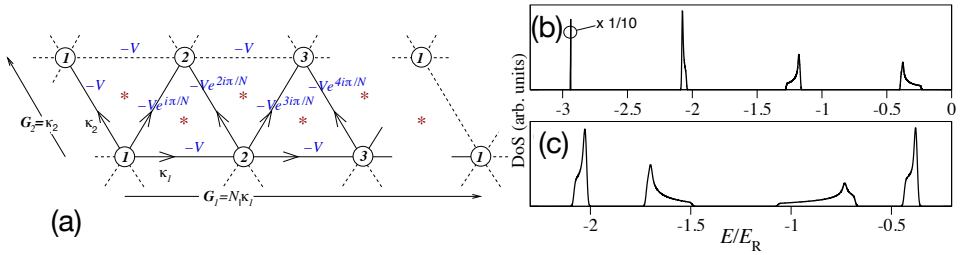

Fig. 3. Generalization of the triangular optical flux lattice for two internal states, Fig. 2, to situations in which N_{I} internal states are coupled. (a) The action of the optical fields on the atoms can be represented by a lattice in reciprocal space: the sites are labeled by the undressed internal states $\alpha = 1, 2, \ldots N_{\mathrm{I}}$ and the displacements represent momentum transfers. The (complex) amplitude linking two sites α, α' of this lattice with momentum transfer $\boldsymbol{\kappa}$ represents the matrix element $V_{\boldsymbol{\kappa}}^{\alpha'\alpha} = \langle \alpha', \boldsymbol{q} + \boldsymbol{\kappa}|\hat{V}_{\mathrm{RWA}}|\alpha, \boldsymbol{q}\rangle$. Here, the reciprocal space unit cell has an area that scales with the number of internal states N_{I}. (b) The resulting energy bands can be made to closely approximate Landau levels, appearing as narrow peaks in the density of states (DoS), here shown for $N_{\mathrm{I}} = 4$ internal states. (c) For a related model, in which the phases on all the optical couplings are doubled, the lowest energy band has Chern number $\mathcal{C} = 2$, but still has narrow width in energy. Reproduced from Ref. 21.

triangular optical flux lattice to N_{I} internal states. Note the expanded BZ, with area that scales with the number of internal states N_{I}. A similar picture is helpful in understanding strongly correlated phases on topological lattices.[22]

The momentum space picture allows flexible design of optical lattices: (i) with low-energy bands that closely approximate uniform Landau levels, having near uniform Berry curvature in reciprocal space, e.g. Fig. 3(b); (ii) in situations in which there is vanishing net flux through the real space unit cell, yet the lowest energy

band has non-zero Chern number, albeit with lattice effects that cause strong varia-
tions in the Berry curvature; (iii) with a lowest energy band that has Chern number
with magnitude larger than unity, Fig. 3(c). Quite generally, one finds that the low
energy bands are topological for a wide range of lattice depth, both for weak lattices
$\mathcal{V}_0/E_R \ll 1$ where the bands can be viewed in a "nearly-free electron" approach and
for $\mathcal{V}_0/E_R \gg 1$ where a tight-binding model is suitable. The ratio of the band width
to band gap is typically minimized for intermediate lattice depths, $\mathcal{V}_0/E_R \sim 1$, and
can be made very small. For example, the lowest band of Fig. 3(b) has a width
$\lesssim 0.005E_R$ which is about 200 times less than the gap to the next energy band.

The practical implementation of these methods requires careful choice of internal
levels and of the light fields causing the optical coupling.[23] This is particularly
true for cases using $N_I > 2$ internal levels, since (electric dipole) selection rules
impose important restrictions on the allowed couplings. For example, a practical
method by which one can form optical flux lattices using the $N_I = 3$ spin states
of rubidium-87 involves radio-frequency dressing of the atomic levels into three
non-uniformly spaced states, which are then coupled by two-photon transitions
in a complex light field involving nine frequency components.[24] Quite generally,
the optical flux lattices operate at high flux densities, $n_\phi \sim N_I/\lambda^2 \sim N_I\kappa^2$. The
interaction energy scale for fractional quantum Hall states with $n_{2D} \sim n_\phi$ can be
relatively large, i.e. $\mu = g_{2D}n_{2D} \sim (a_s/a_z)N_I E_R$, with the recoil energy of order
$E_R/h \sim 3$kHz. Moreover, owing to the very narrow energy bands (with width a
small fraction of E_R), this interaction energy can be made large compared to the
bandwidth even for modest values of a_s/a_z, leading to the possibility of strongly
correlated phases.[24]

2.1.3. *Tight-binding lattices*

In the previous sections we have considered atoms that are moving continuously
in real space, and subjected to relatively weak external potentials that are used
to introduce effective magnetic fields. We were driven towards considering atoms
in optical flux lattices, for which the optimal properties arise for relatively shallow
lattices $\mathcal{V}_0 \sim E_R$.

Here we consider lattices in the limit in which the potential is sufficiently deep
$\mathcal{V}_0 \gtrsim E_R$ that the low-energy bands can be viewed within a tight-binding descrip-
tion. This leads to the connection to tight-binding models that are familiar from
solid state systems. In order to construct topological bands, with non-zero Chern
number, one needs to break time-reversal symmetry in the tight-binding model.
Thus, the goal of the methods described here is to generate inter-site tunnelling
matrix elements with non-zero Peierls phase factors, corresponding to the gener-
ation of (local) orbital magnetic fields which break this symmetry. For simplicity
we shall focus on settings in which the potentials are scalar and the atoms have no
internal spin degrees of freedom. However, the ideas presented here can be married
with spin-changing processes.[25,26] Indeed a recent experiment has realized a Chern
band using the techniques of Sec. 2.1.2 within a tight-binding regime.[27]

The methods used to generate topological Chern bands in such tight-binding settings all fall in the class of "Floquet" systems, in which the Hamiltonian is made to vary in time in a periodic matter.[28] When the period T is sufficiently short, such that $\hbar\omega = h/T$ is much larger than other relevant energy scales in the system, the time evolution at long times can be understood in term of the effective Floquet Hamiltonian, H_{eff}. This is defined by the evolution operator over one period, given by the time-ordered integral $\mathcal{T}\exp[-\frac{\mathrm{i}}{\hbar}\int_{t_0}^{t_0+T} H(t')\mathrm{d}t'] \equiv \exp(-\mathrm{i}H_{\text{eff}}T/\hbar)$. The methods used fall into two broad categories, depending on whether the frequency $\omega \equiv 2\pi/T$ of the time-varying part of the Hamiltonian is resonant or non-resonant with transitions in the spectrum of the static part of the Hamiltonian.

Non-resonant modulation. For non-resonant modulation, and at frequencies that are sufficiently large, the effective Floquet Hamiltonian can be constructed through the application of the Magnus expansion.[28] This expresses the Floquet Hamiltonian as a power law series in $1/\omega$, with a leading term that is the time-averaged Hamiltonian. An important example of this approach is provided by circular shaking of a honeycomb lattice,[29] in which the lattice is displaced by $\boldsymbol{R}(t) = R_0(\cos\omega t, \sin\omega t)$. In the frame of reference that moves with the lattice, the shaking appears as a force $\boldsymbol{F}(t) = -M\ddot{\boldsymbol{R}}(t)$, and the Hamiltonian may be written

$$H(t) = -J_0 \sum_{\langle i,j \rangle} b_i^\dagger b_j - \boldsymbol{F}(t) \cdot \sum_i \boldsymbol{r}_i b_i^\dagger b_i , \qquad (16)$$

where the sites i are arranged on a honeycomb lattice at positions $\boldsymbol{r}_i$, and $\langle i,j \rangle$ denotes the sum over all nearest neighbor pairs. The effective Hamiltonian is equivalent to the tight-binding model of graphene subjected to circularly polarized radiation.[30] Applying the Magnus expansion up to first order in $1/\omega$ leads to an effective Floquet Hamiltonian in which there is a correction to the nearest-neighbor tunnelling amplitude, $J_0 \to J$, and the appearance of a *second*-neighbor tunnelling with an imaginary amplitude[11]

$$H_{\text{eff}} = -J \sum_{\langle i,j \rangle} b_i^\dagger b_j - \mathrm{i}J' \sum_{\langle\langle k,l \rangle\rangle} b_k^\dagger b_l . \qquad (17)$$

This directly realizes the Haldane model,[31] in which time-reversal symmetry is broken by second-neighbor tunnellings (here denoted by double angled brackets). Since the Peierls phase factor generated for second neighbor coupling is $\varphi = \pi/2$ the model is in a regime suitable for the formation of topological bands. This approach was implemented for fermionic atoms in the experiments of Ref. 29, and evidence of the non-zero Berry curvature of the bands was obtained from measurements of the anomalous velocity.

Resonant modulation. A very flexible way in which to imprint tunnelling matrix elements with non-zero Peierls phase factors is to use resonant modulation, or photon-assisted tunnelling.[25] The method is based on taking a static Hamiltonian

in which neighboring lattice sites are offset in energy by an amount Δ that is much larger than the inter-site tunnelling matrix element. For example, a strong linear potential gradient in a one-dimensional lattice leads to

$$H_0^{1D} = -J_0 \sum_j \left(b_j^\dagger b_{j+1} + b_{j+1}^\dagger b_j \right) + \sum_j \Delta j b_j^\dagger b_j \,. \tag{18}$$

For $\Delta \gg J_0$ the energy eigenstates are strongly localized at individual lattice sites. Inter-site motion between two neighboring sites is restored by adding a potential difference between the sites that varies at the resonant frequency $\omega = \Delta/\hbar$. For such resonant coupling, one can apply the RWA, provided the frequency ω is large compared to all other relevant frequency scales, to give a resulting time-independent Hamiltonian. The phase of the resulting tunnelling matrix element can vary in space if there are spatial variations in the relative phases of the modulating potentials. In practice this can be achieved by a two-photon process, with Δ the beat frequency between two light beams, which generate a running wave potential, $H^{1D}(t) = H_0^{1D} + V_0 \sum_j \cos(\Delta t/\hbar + j\varphi)$. The resulting phase of the modulation varies in space in a linear manner

$$H_{\text{RWA}}^{1D} = -J \sum_j \left(e^{i\varphi j} b_j^\dagger b_{j+1} + e^{-i\varphi j} b_{j+1}^\dagger b_j \right) \,, \tag{19}$$

with $J \sim J_0(V_0/\Delta)$.[11] Extending this to a 2D model, in which every row along x is described by the above hopping and in which hopping along y occurs naturally with (real) amplitude J leads to a realization of the (isotropic) Harper–Hofstadter model:[32] hopping on a square lattice with $n_\phi = \varphi/2\pi$ flux quanta in each plaquette. This leads to the spectrum of the Hofstadter butterfly,[33] with a complex set of energy bands which have, in general, non-zero Chern numbers,[20] Fig. 4.

Using this, and related, techniques of resonant modulation, the Harper–Hofstadter model has been implemented in experiments with flux $n_\phi = 1/4$[34,35] and with $n_\phi = 1/2$.[36] Recent experiments have studied the motion of small numbers of particles on a Harper–Hofstadter lattice in a quantum gas microscope with single site resolution.[37] Characteristic energy scales are set by the intersite coupling J, and the onsite interaction energy, U, which can readily be in a strong coupling regime $U \gg J$.

2.2. *Many-body phases*

In the preceding section we have described ways in which cold atoms can be made to experience effective magnetic fields, leading to the formation of Landau levels or other topological energy bands. We now turn to discuss the many-body phases of interacting bosons that occupy these single-particle states. We separate the discussion into two parts: first for interacting bosons in continuum Landau levels associated with a uniform magnetic field, as generated by rotation in a harmonic trap; second for situations in which the atoms experience a periodic lattice potential. For the most part, we shall put the emphasis on the properties of thermodynamically
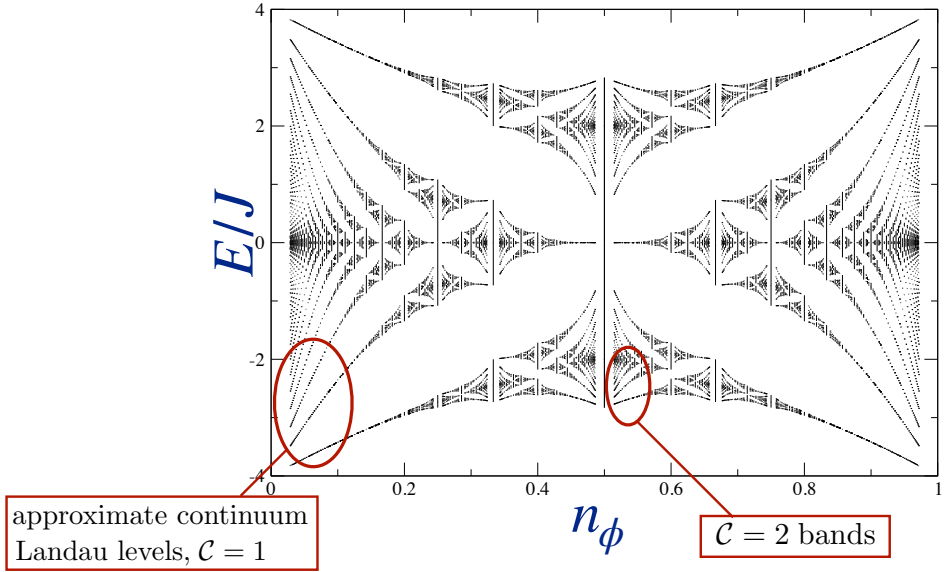
Fig. 4.   Hofstadter butterfly energy spectrum of the Harper–Hofstadter model with tunnelling energy J. For flux $n_\phi \ll 1$ the low energy bands recover the continuum Landau levels, each of Chern number $\mathcal{C} = 1$. For n_ϕ close to $1/q$ the low energy bands each have Chern number $\mathcal{C} = q$, indicated here for $\mathcal{C} = 2$ close to $n_\phi = 1/2$. Figure courtesy of G. Möller.

large systems where clear statements can be made regarding the nature of the ground state phase, albeit through the analysis and extrapolation of the results of numerical studies of systems of small numbers of particles.

2.2.1.   Interacting bosons in the lowest Landau level

Consider a system of N (spinless) bosons in 2D with contact interactions

$$H = \sum_{i=1}^{N} \frac{(\boldsymbol{p}_i - M\boldsymbol{\Omega} \times \boldsymbol{r}_i)^2}{2M} + g_{2\mathrm{D}} \sum_{i<j=1}^{N} \delta(\boldsymbol{r}_i - \boldsymbol{r}_j)\,. \tag{20}$$

This can be achieved for a rotating gas in a trap when the rotation frequency Ω matches the trap frequency ω_0. For $\Omega < \omega_0$ there is a residual harmonic potential $(1/2)M(\omega_0^2 - \Omega^2)|\boldsymbol{r}|^2$ which provides an overall residual confinement, Eq. (4). For clarity we omit consideration of this confinement, but note that in general it will lead to an overall non-uniform density distribution.

In the following we describe the nature of the many-body ground states for bosons in the lowest Landau level. Since we are dealing with contact interactions (20), there is only one non-zero Haldane pseudo-potential[38]

$$V_0 = \sqrt{\frac{2}{\pi}} \frac{\hbar^2 a_s}{M a_0^2 a_z} \sim \hbar\omega_0 \frac{a_s}{a_z}\,, \tag{21}$$

the interaction energy of two particles with zero relative angular momentum. For the most part we shall focus on the ground states of bosons with this simple contact interaction. However, we note that longer-range interactions can be relevant for atoms with dipolar interactions,[8] which contribute to all V_m with even m.

Laughlin State. For a gas of N contact-interacting bosons, rotating at high angular momentum in an isotropic parabolic trap, the $\nu = 1/2$ Laughlin state

$$\Psi^{\mathrm{L}}_{q=2}(z_1, z_2, \ldots, z_N) \propto \prod_{i<j=1}^{N} (z_i - z_j)^2 e^{-\sum_i |z_i|^2/4} , \qquad (22)$$

is the exact ground state[13] at total angular momentum $L = N(N-1)$. This result arises from the fact that, for this value of the angular momentum, it is the unique bosonic wave function in the lowest Landau level that vanishes when any pair of particles coincide. Thus, at sufficiently high rotation rate one anticipates that the cold atomic gas will realize this fractional quantum Hall state. This expectation is, of course, borne out in numerical calculations, not only in the disk geometry, Eq. (22), but also in edgeless geometries of the sphere and the torus which are most useful for determining the bulk properties. Figure 5 shows the excitation spectrum for the $\nu = 1/2$ state on a torus. From such studies the bulk gap for creation of a quasi-particle/quasi-hole pair of $\Delta E_{\nu=1/2} \simeq 0.095(5) \times 2\pi V_0$ can be extracted.[10] It is worth noting that the quasi-holes have exactly zero interaction energy for the situation considered, of contact interactions. Thus the quasi-holes behave as
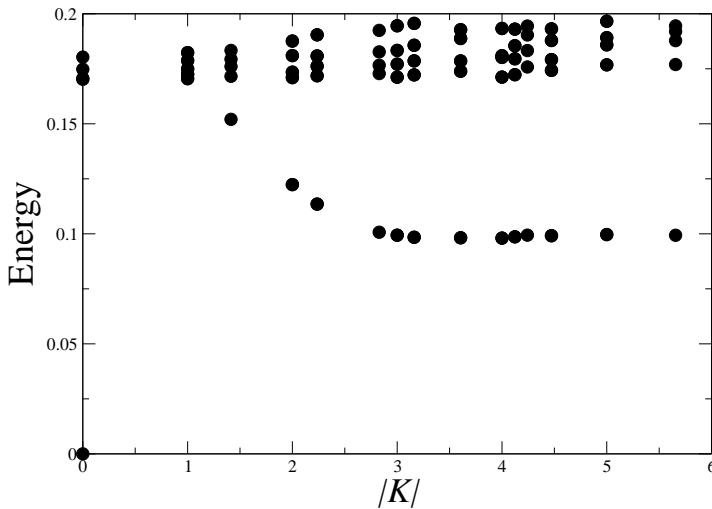

Fig. 5. Excitation spectrum of the $\nu = 1/2$ Laughlin state of bosons with contact repulsion. Computed on a torus for $N = 8$ particles in $N_\phi = 16$ flux quanta. The ground state (two-fold degenerate) is at $E = 0$ and $\boldsymbol{K} = 0$. Energies are measured in units of $2\pi V_0$, with V_0 the Haldane pseudo-potential, Eq. (21), and lengths in units of the magnetic length, ℓ_B.

ideal fractionalized excitations, with vanishing interactions. Indeed, at $\nu < 1/2$, or equivalently $L > N(N-1)$, there are multiple ground states, all with vanishing interaction energy, and with a degeneracy associated with the fractional exclusion statistics of the Laughlin quasi-holes. We shall come back to this in connection with their possible experimental consequences in Sec. 2.3.

That the $\nu = 1/2$ Laughlin state is the exact ground state of a gas of bosons in this experimentally relevant setting — contact interactions, parabolic trap and (potentially) small numbers of particles — is a central result that underpins the expectations that cold atomic gases can be brought to regimes in which fractional quantum Hall physics emerges.

Vortex Lattice. It is helpful to compare the Laughlin state with the vortex lattice phase of a superfluid that is subjected to low, or moderate, rotation rates. Since particle velocity in a superfluid is proportional to the gradient of the phase, the curl of the velocity field vanishes except at singular points — the vortex cores — at which there is a delta-function contribution of strength set by the quantized circulation $\kappa = h/M$. In a uniform setting (e.g. where a potential acts to counterbalance the centrifugal potential) the steady state in the rotating frame consists of a lattice of these quantized vortices, with the density of vortices, n_{v}, set by Feynman's condition that the mean circulation matches that of rigid body rotation $\boldsymbol{v} = \boldsymbol{\Omega} \times \boldsymbol{r}$, i.e. $n_{\mathrm{v}}(h/M) = \boldsymbol{\nabla} \times (\boldsymbol{\Omega} \times \boldsymbol{r}) = 2\Omega$, that is $n_{\mathrm{v}} = 2\Omega M/h$. Thus, the density of vortices in the vortex lattice is equal to the density of flux quanta (5) of the effective magnetic field (1) associated with the rotation. Indeed this is borne out, even for weakly interacting bosons, in detailed numerical simulations of the vortex distribution.[39] The hydrodynamic behavior of the vortex lattice in the lowest Landau level has been studied in Refs. 40 and 41.

The mean-field vortex lattice phase treats the vortices as classical objects. Going beyond this, to include quantum fluctuations of the vortices, shows that the vortices have a quantum uncertainty in position which is of order the mean inter-particle spacing $\bar{a} = n^{-1/2}$ where n is the 2D density of the bosons.[42] This result expresses the very natural expectation that one cannot locate the core of the vortex to an accuracy better than the inter-particle spacing. Applying a Lindemann criterion for these fluctuations, one asserts that the vortex lattice is stable when the uncertainty in vortex position is smaller than some multiple of the mean vortex spacing, $\bar{n}^{-1/2} < c_L \bar{n}_\phi^{-1/2}$, or equivalently

$$\nu \equiv \frac{n}{n_\phi} > \nu_c \,. \tag{23}$$

That is, the vortex lattice can be a stable ground state at sufficiently high filling factor.[42] This is consistent with analytic results that apply in the limit $\nu \to \infty$.[43] A simple evaluation of the quantum fluctuations in the vortex lattice leads to $\nu_c \simeq 7$,[42] while an alternative definition, and more detailed calculation, leads to a critical filling factor of $\nu_c = 17$.[40] However, both of these estimates rely on the use of an

unknown Lindemann parameter, c_L. Direct calculations of the critical filling factor ν_c have been performed using exact diagonalization for contact interacting bosons on a toroidal geometry. These calculations indicate a transition to a ground state with broken translational invariance, consistent with that of the triangular vortex lattice, at $\nu_c \simeq 6$.[42] Subsequent numerical calculations showed that strong density wave correlations persist down to $\nu = 2$.[44] Thus, the existing numerics suggest a critical filling factor above which the vortex lattice is the ground state of $\nu_c \simeq 2-6$ for contact interactions in the lowest Landau level. These numerics are restricted to very small systems, so are subject to strong finite-size effects.

Composite Fermion States. That the ground state is a vortex lattice at $\nu > \nu_c$ and is the Laughlin liquid at $\nu = 1/2$ leaves open the question of what are the phases in the range $1/2 < \nu < \nu_c$. Early numerical work showed evidence for a successful description of the many-body states in this regime in terms of composite fermions.[45] Here, the composite fermions are formed by binding each boson to a single vortex of the many-body wave function, such that the flux density experienced by the composite fermions is

$$n_\phi^{\mathrm{CF}} = n_\phi - n \,. \tag{24}$$

Treating the composite fermions as non-interacting particles, one expects an incompressible integer quantum Hall state of the composite fermions when p Landau levels are filled, $n/n_\phi^{\mathrm{CF}} = \pm p$, leading to the Jain sequence[46]

$$\nu = \frac{p}{p \pm 1} \,. \tag{25}$$

In addition to the Laughlin state at $\nu = 1/2$, numerical studies on the sphere and the torus have shown evidence for gapped states at $\nu = 2/3$ and $\nu = 3/4$.[42,47] However, there appear to be significant interactions between the composite fermions, so higher members of this sequence do not appear as ground states. Furthermore, as discussed below, the composite fermion states at $\nu = 2, 3/2$ do not appear to describe the ground states of contact interacting bosons at these filling factors.

Moore–Read State. At $\nu = 1$ a model of non-interacting composite fermions would suggest the existence of a *compressible* composite Fermi liquid, analogous to the $\nu = 1/2$ state of fermions.[48] This compressible state is the $p \to \infty$ limit of the sequence (25). This is not found in numerics. Rather the ground state is found to be a robust gapped FQH state. Numerical studies have established this state to be well described by the Moore–Read Pfaffian state,[49] with a particle-hole gap of $\Delta E_{\nu=1} \simeq 0.05 \times 2\pi V_0$.[10,42,47] Note that this is not significantly smaller than the gap for the $\nu = 1/2$ Laughlin state ($\Delta E_{\nu=1/2} \simeq 0.095 \times 2\pi V_0$), indicating that the Moore–Read state is of comparable robustness. Numerical evidence for the Moore–Read state appears from the shift on the sphere, the expected three-fold degeneracy of the ground state on the torus, and adiabatic continuity with the Moore–Read

wavefunction which is the exact ground state of a three-body contact interaction. Unlike electrons in the lowest Landau level at $\nu = 1/2$, bosons in the lowest Landau level at $\nu = 1$ do not have an exact particle-hole symmetry. The competition with the possible anti-Pfaffian wavefunction is resolved in favor of the Moore–Read Pfaffian for contact interacting bosons at $\nu = 1$. That this non-Abelian FQH state appears so robustly in the bosonic system is a key motivation for searching for experimental realizations of fractional quantum Hall states of bosons.

Read–Rezayi States. Even more interesting are the ground states that appear at filling factors larger than $\nu = 1$. Numerical studies show that the ground states of contact interacting bosons in the lowest Landau level at $\nu = k/2$, with $k \geq 3$ integer, resemble the Read–Rezayi states.[42] For bosons these can be defined as the states of highest filling factor in the lowest Landau level which are the exact zero energy eigenstate of a $(k+1)$-body contact interaction.[50] They generalize the Laughlin and Moore–Read states, which are respectively the $k = 1$ and $k = 2$ members of the sequence. For N divisible by k, the states can be written as a symmetrized product over k Laughlin states[42,51]

$$\Psi_k^{\mathrm{RR}}(z_1, z_2, \ldots, z_N) \propto \mathcal{S}\left[\prod_{i<j \in A}^{N/k} (z_i - z_j)^2 \prod_{k<l \in B}^{N/k} (z_k - z_l)^2 \ldots \right] e^{-\sum_i |z_i|^2/4}, \quad (26)$$

where $\mathcal{S}$ denotes symmetrization over all ways in which the N particles can be divided into sets $A, B, \ldots$ of N/k particles. The wavefunction (26) vanishes when $k+1$ particles coincide since at least two of these particles (i and j, say) must be in the same set, and therefore the wavefunction has a factor of $(z_i - z_j)^2$. Like the Moore–Read state the Read–Rezayi states describe non-Abelian phases of matter. However, the relevant anyons step beyond the Ising non-Abelian anyons of the Moore–Read state to allow universal braid statistics.[52]

For contact interactions, the correlation lengths are large, and there are competing phases with broken translational order already for $\nu \geq 2$. (These competing phases include both vortex lattice and stripe/nematic phases.[44]) However, it has been shown that the addition of a small degree of longer-range interaction (i.e. a non-zero Haldane pseudo-potential V_2) can improve stability.[53] This is illustrated for the $k = 3$ Read–Rezayi state in Fig. 6. Recall that there is a competing composite fermion state (25) at $\nu = 3/(3-1) = 3/2$. Nevertheless, the numerical results — in particular the four-fold ground state degeneracy — indicate that this state is not favored compared to the $k = 3$ Read–Rezayi state under the conditions of Fig. 6.

In cold atom experiments, longer-range interactions may arise in atomic species with large dipole moments.[8] These longer-range interactions can also lead to changes in the nature of the vortex lattice phases,[54] and/or the appearance of competing crystalline phases.[55]

Fermions. Although the focus of this chapter is on bosons, we note that there are some aspects of the FQH state of fermionic atoms that are unconventional.
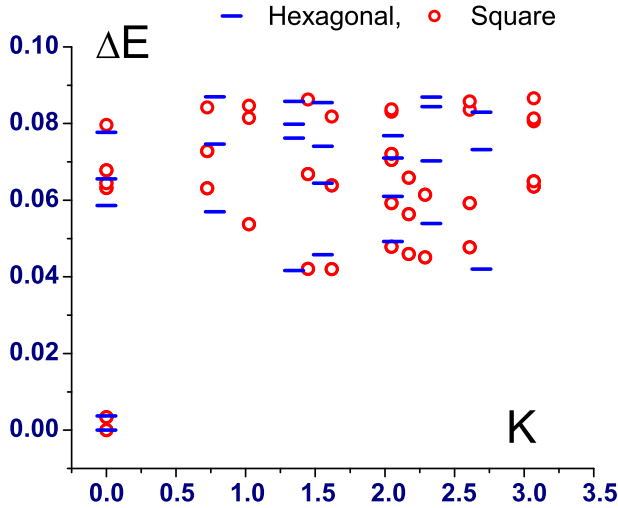
Fig. 6. Excitation spectrum at $\nu = 3/2$ for $N = 13$ bosons on the torus for non-zero range of the interaction giving Haldane pseudo-potential ratio $V_2/V_0 = 0.38$. The near degeneracy of the two levels at $\boldsymbol{K} = 0$ is as expected for the $k = 3$ Read–Rezayi state. (There is an overall four-fold degeneracy when translational symmetries are taken into account.) The insensitivity to boundary conditions on the torus illustrates convergence. Reproduced from Ref. 53.

Most notable is the availability of gases of two-component fermions for which the superfluid pairing of the fermions can be controlled: spanning the weakly attractive "BCS" regime of Cooper pairs of size large compared to the inter-particle spacing, to the regime of strong binding of pairs into tightly bound bosons of small size which then form a Bose–Einstein condensate (BEC).[5] This leads to interesting possibilities involving the interplay between fermionic pairing and fractional quantum Hall states. For a homogeneous gas without external magnetic field, the transition in the form of ground state is known to be a smooth evolution between BCS and BEC regimes. However, in the presence of a quantizing magnetic field — for which the ground states can have character of the quantum Hall states in 2D, or layered QH states in 3D — one can readily establish that these two limits must be separated by a phase transition.[56] This is most evident for a 2D system of two-component fermions of density n^F at flux n_ϕ^F with filling factor $\nu^F = n^F/n_\phi^F = 2$. For weak attractive interactions between the two components, the ground state is a $\nu^F = 2$ integer quantum Hall state in which the lowest Landau level is filled for both spin components. However, for very strong attractive interactions such that opposite spin fermions pair into bosons with binding energy large compared to the cyclotron energy, the system should be viewed as bosons of density $n^B = n^F/2$ experiencing a flux density $n_\phi^B = 2n_\phi^B$, i.e. at filling factor $\nu^B = \nu^F/4 = 1/2$. Residual contact repulsion between the bosons will stabilize a Laughlin state of these bosons. That there must be a phase transition separating these two regimes is evident from the

fact that the edge structure changes: from two modes for the integer quantum Hall state of weakly attractive fermions at $\nu^{\mathrm{F}} = 2$ to the single mode of the Laughlin state of bosons at $\nu^{\mathrm{B}} = 1/2$.[56–58]

2.2.2. *Interacting bosons in topological optical lattices*

A key feature of optical lattices is that they break continuous translational invariance. Thus, in order that strongly correlated phases akin to FQH states appear in these lattices, one must go beyond the paradigm of continuum Landau levels to allow for this discrete translational invariance. That fractional quantum Hall states can be stable in the presence of periodic density modulations was discussed in early work on the "Hall crystal" phase, in which the density order is spontaneously formed.[59] The consequences of the discrete translational invariance on the form of the Chern–Simons field theoretical description of the Laughlin and Jain states were studied.[60] More recently, this topic has gained attention in connection with the investigation of "fractional Chern insulators"[61–63] — i.e. fractional quantum Hall states formed for particles moving in lattice models which generate bands with non-zero Chern number, with single particle wavefunctions that can differ markedly from those of the continuum Landau level. The optical lattices described in Sec. 2.2.2 provide interesting examples of this physics. Similar effects have been observed for electrons in superlattice structures formed in bilayer-graphene hexagonal boron-nitride devices.[2]

$\mathcal{C} = 1$ **bands.**   Many of the optical lattices described above have been designed to closely approximate the action of a uniform magnetic field on a charged particle, and thereby to form energy bands that are similar to those of Landau levels. This is the case for the Harper–Hofstadter model at sufficiently small flux per unit cell, n_ϕ, where the magnetic length is much larger than the lattice constant. It is also the case for the optical flux lattices of Sec. 2.1.2. In such cases, one expects that the many-body states for short-range interactions will mirror those described above for contact-interacting bosons in the lowest Landau level — at least in regimes for which the mean interaction strength remains sufficiently small to preclude inter-band mixing. Although the energy bands can be similar to Landau levels, they are not identical: the bands have some residual dispersion, and the Berry curvature of the energy band is not uniform. Therefore it is important to test the stability of quantum Hall states in the continuum to these settings.

The nature of the ground states of interacting bosons on the Harper–Hofstadter model have been studied using numerical methods, both for hardcore interactions and for contact interactions that do not mix states beyond the lowest energy single-particle band. The results of these studies[64,65] show that the ground state at filling factor $\nu = 1/2$ remains well-described by the Laughlin state for $n_\phi \lesssim 0.3$, as does the composite fermion (25) state at $\nu = 2/3$.[66,67] These states are evidenced by the presence of energy gaps, by the appropriate ground state degeneracies on a
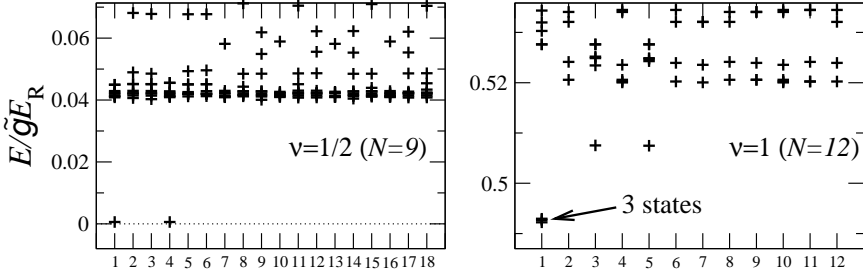
Fig. 7. Many body excitation spectra for bosons in the lowest band of an optical flux lattice designed to mimic the lowest Landau level, using $N_I = 3$ hyperfine levels of rubidium-87. (a) At $\nu = 1/2$ ($N = 9$ particles in $N_\phi = N_1 N_2 = 6 \times 3$ states) the ground state is well described by the Laughlin state, with two-fold degeneracy (b) At $\nu = 1$ ($N = 12$ particles in $N_\phi = N_1 N_2 = 6 \times 2$ states) the ground state is well described by the Moore–Read state, with three-fold degeneracy. Energies are measured in units of $\tilde{g}E_R = 3\sqrt{2\pi}(a_s/a_z)(\hbar^2\kappa^2/m)$ (with κ the characteristic wavevector of the light forming the optical lattice), and the momentum $\boldsymbol{k} = \alpha_1 \boldsymbol{G}_1/N_1 + \alpha_2 \boldsymbol{G}_2/N_2$ is labeled by the index, $i = 1 + \alpha_1 + N_1\alpha_2$, with $\boldsymbol{G}_{1,2}$ the two smallest reciprocal lattice vectors. Reproduced from Ref. 24.

torus, and by the many-body Chern numbers. The connection with the FQH states of the continuum Landau levels has been explored in Ref. 68, showing how non-uniformities of the geometry of the Bloch wave functions affect the stability of the FQH states.

The optical flux lattices, described in Sec. 2.1.2, allow the formation of bands that closely approximate Landau levels. The Laughlin ($\nu = 1/2$) and Moore–Read ($\nu = 1$) states were studied in detail for the model of Fig. 3(a) for $N_I = 3, 4$, and were shown to have similar stability to that found in the continuum Landau levels.[69] Focusing on settings in which the bands closely mimic Landau levels, but with an eye on specific practical implementation for the $N_I = 3$ spin states of rubidium-87, a scheme similar to that illustrated in Fig. 3(a) was proposed.[24] This scheme sacrifices uniformity of the Berry curvature of the band to simplify the experimental implementation. The resulting energy bands can still be made very narrow. However, they are of non-zero width and so sufficiently strong interactions are needed to prevent formation of a Bose–Einstein condensate in the lowest energy band minimum (or superposition of degenerate minima). At strong interactions one finds the appearance of a robust Laughlin state at $\nu = 1/2$ and a robust Moore–Read phase at $\nu = 1$, much as in continuum Landau levels. These studies show good prospects for finding the FQH states of bosons of continuum Landau levels within the setting of optical lattices, where densities and interaction energies can be large.

Much is known concerning the interacting ground states in other flat-band models with topological bands.[61,63] Typically such models are formulated as tight-binding models with further neighbor couplings introduced to reduce the bandwidth, and are therefore less readily implemented in cold atom systems. It is interesting to note that, by careful choice of these further neighbor couplings, the wavefunctions

can be made identical to those of the continuum Landau level,[70] allowing the development of a model in which a discretized version of the Laughlin wavefunction[71] is the exact many-body ground state.

$\mathcal{C} \neq 1$ **bands.**   The optical lattices described above also provide settings in which the lowest energy band differs qualitatively from a continuum Landau level, by having a Chern number that is not of unit magnitude, $|\mathcal{C}| \neq 1$. For example, as discussed in more detail below, such cases arise for the Harper–Hofstadter model with n_ϕ close to $1/q$, for which the lowest energy band has Chern number $|\mathcal{C}| = q$. For interacting bosons occupying this lowest energy band, one can anticipate strongly correlated phases provided the interaction energy is large compared to the bandwidth. How do these states, formed in Chern bands with $|\mathcal{C}| \neq 1$ relate to fractional quantum Hall states in continuum Landau levels? Remarkably one can gain understanding in this setting by adapting ideas of composite fermion theory to this lattice setting.

The extension of the mean-field composite fermion theory of the continuum Landau levels to the lattice was described in Ref. 60, and explored numerically for contact interacting bosons in Refs. 66, 67 and 72. For bosonic particles, one may form composite fermions by attaching a single vortex. As in the continuum theory, the effective flux density is $n_\phi^{\mathrm{CF}} = n_\phi - n$, Eq. (24). For n and n_ϕ of small magnitude, the relevant single-particle states are approximate continuum Landau levels both for n_ϕ and for n_ϕ^{CF}. The resulting many-body states recover the continuum composite fermion states described above, with bosonic Jain sequence Eq. (25). However, when either n or n_ϕ is of order unity, such that the lattice structure becomes significant, then n_ϕ^{CF} may not be small and the levels that the composite fermions fill can have different character to those of the continuum Landau level.

We illustrate the general approach here by the specific example of the Harper–Hofstadter model at flux n_ϕ close to $1/q$ with q being an integer. In each of these cases, there appears a series of narrow low energy bands in the spectrum which are well separated from each other in energy. For $q = 1$ this condition is equivalent to n_ϕ being close to zero and these narrow bands are the usual Landau levels. These continuum Landau levels and the low energy bands associated with proximity to $n_\phi = 1/2$ are illustrated in Fig. 4.

The low-lying bands of the Harper–Hofstadter model close to $n_\phi = 1/q$ have Chern number $\mathcal{C}$ of magnitude $|q|$. One way to see this is to use a result of Wannier[73] who showed that the number of states per plaquette for each of these bands is $n_s = |q n_\phi - 1|$. By considering one such band to be filled by non-interacting fermions, such that $n = n_s$, and using the Středa formula[74]

$$\sigma_{xy} = e \left(\frac{\partial n}{\partial B} \right)_\mu = \frac{e^2}{h} \left(\frac{\partial n_s}{\partial n_\phi} \right)_\mu = \pm q \frac{e^2}{h} \text{ for } n_\phi \gtrless 1/q \qquad (27)$$

one deduces that the Chern number of the band is $\mathcal{C} = |q|$. Alternatively, one can consider the sequence $n_\phi = \alpha / [|\mathcal{C}|\alpha - \mathrm{sgn}(\mathcal{C})]$ with integer α, which converges

to $n_\phi = 1/|\mathcal{C}|$ at large α. Solving the Diophantine equation of Thouless *et al.*[20] at these flux densities to determine the Hall conductance of the low energy bands shows that they each have Chern number $\mathcal{C}$.[72]

Consider the lowest such band occupied with a density n of repulsively interacting bosons. Given that the band consists of n_s states per unit area, it is natural to define the filling per *state* by $\nu_s \equiv n/n_s$. We use the subscript s to emphasize that this is the filling per state rather than per flux quantum, $\nu = n/n_\phi$. (For models that realize bands that closely approximate Landau levels, then $\nu_s = \nu$.) Now consider forming composite fermions by attaching a single vortex, such that a density n of composite fermions experience a resulting flux density $n_\phi^{\text{CF}} = n_\phi - n$. If also $n_\phi^{\text{CF}} \simeq 1/|\mathcal{C}|$, which always applies for low densities $n \ll 1$, these composite fermions will experience low energy $|\mathcal{C}|$ bands of the same form as the original bosons. The number of states per unit area is $n_s^{\text{CF}} = |\mathcal{C} n_\phi^{\text{CF}} - 1| = |\mathcal{C}(n_\phi - n) - 1|$. Treating the composite fermions as non-interacting, one would expect an incompressible state when p bands are filled, $n = \pm p n_s^{\text{CF}}$, leading to the lattice composite fermion sequence[72]

$$\nu_s \equiv \frac{n}{n_s} = \frac{p}{p\mathcal{C} \pm 1}. \tag{28}$$

This generalizes the Jain sequence (25) for conventional Landau levels to the case of topological bands with $|\mathcal{C}| \neq 1$. Numerical exact diagonalizations show evidence for the existence of these states for $\mathcal{C} = 2$[66,72] and $\mathcal{C} = 3$.[72] The same reasoning leads to candidate fermionic states in bands at $\nu_s = \frac{p}{2p\mathcal{C} \pm 1}$;[72] evidence for such a state in a $\mathcal{C} = 2$ band has been found in experimental studies of modulated bilayer graphene.[2]

An interesting case appears for $\mathcal{C} = 2$ and $p = 1$, for which there is a composite fermion state with $\nu_s = p/(2p - 1) = 1$. This state is a bosonic *integer* quantum Hall (BIQH) state. It has no fractionalized excitations (i.e. it has a non-degenerate ground state on a torus) so has short-range entanglement. It is therefore an example of a symmetry-protected topological phase of bosons,[75] the symmetry being the $U(1)$ symmetry associated with conservation of particle number. Consistent with general arguments[76] this state has *even* value of the quantized Hall conductance, $\sigma_{xy} = 2e^2/h$. Numerical results show evidence for the stability of this phase for bosons with contact interactions in the Harper–Hofstadter model.[66,67,72]

Optical flux lattices, described in Sec. 2.1.2, can also be designed for which the real space magnetic field vanishes, yet the Chern number is nonzero, or in which the Chern number has magnitude larger than unity.[21] The strongly correlated phases of models in which the lowest band has $\mathcal{C} = 2$ were studied in Refs. 69 and 77. It was shown that various fractional Chern insulator states can appear. These include so-called "color-entangled" states, at fillings $\nu_s = 1/(1 + \mathcal{C})$ at least for $\mathcal{C} = 2$ and $\mathcal{C} = 3$.[69] These states are related to the fractional quantum Hall states of multi-component quantum Hall systems proposed by Halperin,[78] with $\mathcal{C}$ internal components[79] albeit in a setting without SU($\mathcal{C}$) symmetry. However, they differ in detailed structure. These differences can be exposed in finite-size systems,

using an extended zone construction of the form of Fig. 3(a), for which a band of Chern number $\mathcal{C}$ has a number of states that is not divisible by $\mathcal{C}$. Thus, the band cannot be viewed as consisting of $\mathcal{C}$ copies of a band with unit Chern number, so does not have a natural description in terms of $\mathcal{C}$ internal components. Still, the color-entangled fractional Chern insulator states can be well defined even in this case.[22]

2.3. *Experimental consequences*

There remain experimental challenges in realizing FQH states for atomic gases. However, these appear to be technical, and there are rapid ongoing improvements in capabilities which encourage one to believe that they can be overcome. The theoretical studies provide strong motivations to continue this search, in particular to have experimental access to non-Abelian phases, such as the Moore–Read state at $\nu = 1$ for contact interacting bosons, and to explore FQH states that are stabilized by the lattice including the predicted $\nu_s = 1$ symmetry-protected topological phase of bosons. It is therefore important to consider what are the experimental observables that could be used to probe and to characterize these phases.

The observables that can be accessed in cold gases are rather different to those that are commonly used in electronic systems. In the following we list some of the most natural observables for cold gases.

Equation of State. The confinement of atomic gases in harmonic traps typically leads to inhomogeneous particle density across the sample. This can cause difficulties in the interpretation of measured properties that are averaged across the sample. However, it can be a useful feature for extracting the equation of state of the system if local measurements are made. Specifically, if the trapping potential $V(\boldsymbol{r})$ is sufficiently shallow that the local density varies slowly on the microscopic correlation length, then one may take the mean local particle density at a position $\boldsymbol{r}$ to represent the equilibrium density for a local chemical potential $\mu(\boldsymbol{r}) = \mu - V(\boldsymbol{r})$. Making *in situ* measurements of the expectation value of $n(\boldsymbol{r})$ (over repeated experiments) then allows one to deduce the equation of state $n(\mu)$. This "local density approximation" has been put to use in an accurate determination of the equation of state of strongly interacting atomic gases.[80] The incompressible character of fractional quantum Hall states should appear clearly in such measurements, as a form of "wedding cake" density distribution, with plateaus in the density at quantum Hall states for sufficiently low temperatures.[81]

Local correlations. Rather than constructing the expectation value of the particle density through averaging over repeated images, analysis of each individual image can be made. Each image provides the positions of all of the particles (up to uncertainties from noise and imaging resolution), so contains significant information on the local two-particle (or multi-particle) correlations. For rapidly rotating

cases in harmonic traps, the images taken after release of the trap and expansion of the gas give a scaled-up view of the local correlations before expansion.[82] For cold atomic gases formed in "quantum gas microscopes" such images can be taken even *in situ* — with atomic resolution and high fidelity.[16,37] Quantum gas microscopes could also be used to measure correlation functions that can uncover and characterize the gapless edge modes of FQH states.[67] The spatial average of the local two-particle correlation function $\langle n(\boldsymbol{r})n(\boldsymbol{r})\rangle$ can also be obtained by the use of photo-association to convert pairs of atoms in close proximity to molecules.[15]

Transport. Although cold atomic gases are not readily attached to sources and sinks of atomic currents, there are ways in which they can be used to measure transport properties. The use of light beams to shape the cloud into two (large) reservoirs, coupled by a mesoscopic region, has allowed studies of two-point transport properties, including thermo-electrical transport, albeit not yet for systems involving topological bands or phases.[83] The bulk transport of a weakly interacting gas of bosons subjected to the Harper–Hofstadter model at flux $n_\phi = 1/4$ was studied via the motion of the centre of mass of the cloud, allowing a measurement of the Chern number of the lowest band.[84] Using a sum rule, the zero frequency Hall conductivity can be related to the integral over frequencies of the dissipative circular dichroism.[85] This has recently been used to measure the Hall conductivity of non-interacting fermions in the lowest band of the Haldane model.[86]

Spectroscopic probes. Cold atomic gases lend themselves naturally to spectroscopic probes. Bragg spectroscopy, namely a two-photon Bragg scattering process, can be performed with high energy resolution, and with wavevector transfers of order of the inverse optical wavelength, which itself is of order the inverse particle spacing, thereby accessing the full range of relevant momenta.[87] This has been used to measure the (gapless) collective modes of a Bose–Einstein condensate,[88] and the static and dynamic structure factors of strongly interacting phases of fermions.[89] This provides a natural way to probe the (gapped) collective modes of FQH states, such as the roton branch of Fig. 5. Observations of the collective modes of finite-size systems are sensitive to the equation of state of the gas,[90] and could be used to probe the edge structure of FQH states.[91]

Fractionalization. The high degree of control and the potential for precision measurements on cold atomic gases holds promise of finding new ways to probe and detect the particle fractionalization within FQH states of atoms. Precision spectroscopy of rotating atomic clusters has been shown to provide a means to detect Haldane exclusion statistics of quasi-hole excitations.[92] Removing one atom from a finite-size $\nu = 1/2$ Laughlin droplet of bosons leaves the system in an excited state involving two quasi-holes; a count of the number of spectral lines reveals the exclusion statistics of these particles. Although more challenging, it is also possible to

envisage means by which to detect braiding statistics.[93,94] An interesting proposal is to introduce additional "impurity" atoms to which anyons of the background FQH state bind, and which may be separately addressed and controlled.[95–98]

Preparation methods. In considering all of these potential experimental observables, an important concern is the means of preparing the system close to its ground state. Typically, *in situ* cooling is unavailable for cold atoms in the complex settings for which the FQH states might arise, so the natural approach is to consider *adiabatic* paths from a more easily prepared many-body ground state to the FQH state. Such trajectories involve a quantum phase transition — from a short-range entangled phase to the FQH state with genuine topological order — so true adiabaticity is only possible in small finite systems.[67,99,100] Theoretical studies have explored the optimal adiabatic paths for small systems[99,101–103] and the use of dissipative methods.[104] If such methods are not available, for large systems one can hope that non-adiabatic effects on crossing the transition into the topologically ordered phase are not too destructive, as in the phase transition between Mott insulator and superfluid phases of strongly interacting lattice bosons.[105]

3. Other Experimental Settings

In Sec. 2 we considered FQH states of bosons formed in ultracold atomic gases. There are a wide variety of other forms of system in which bosonic degrees of freedom can move, without displacing the underlying atoms: a set of localized atoms or molecules (e.g. on a crystalline lattice) can support local spin-flips or other internal excitation which move as bosons through the static lattice; alternatively, the electromagnetic field itself provides a medium through which photons can propagate. In the following we provide an overview of systems in which these bosonic degrees of freedom may form FQH states. For further details, in particular of the topological bands of single-particle excitations in artificial photonic systems, we refer the interested reader to Refs. 106 and 107.

3.1. *Quantum magnets*

A quantum magnet consisting of spin-$1/2$ degrees of freedom can be readily mapped to a model of hard-core bosons. We take the presence/absence of a boson on a given lattice site r to represent a spin projection $s_r^z = \pm 1/2$, such that the number of bosons on site r is $b_r^\dagger b_r = s_r^z + 1/2$, and define the boson creation and annihilation operators by $b_r^\dagger = s_r^+$, $b_r = s_r^-$. These lead to the commutation relation $[b_r, b_{r'}^\dagger] = \delta_{r,r'}(1 - 2b_r^\dagger b_r)$ which is consistent with the hardcore constraint $(b_r)^2 = (b_r^\dagger)^2 = 0$.

Writing the Heisenberg antiferromagnet in terms of these hardcore bosons

$$H_{\mathrm{AF}} = J \sum_{\langle r,r' \rangle} s_r \cdot s_{r'} = J \sum_{\langle r,r' \rangle} \left[\frac{1}{2}\left(b_r^\dagger b_{r'} + b_{r'}^\dagger b_r \right) + n_r n_{r'} \right] + \mathrm{const.} \qquad (29)$$

shows that it corresponds to both nearest-neighbor tunnelling and nearest-neighbor density interactions. Conservation of the total spin $S^z \equiv \sum_{\boldsymbol{r}} s^z_{\boldsymbol{r}}$ is equivalent to conservation of the total number of bosons. Similarly an external field B^z that couples to S^z plays the role of a chemical potential.

Kalmeyer and Laughlin[4] proposed that the groundstate of the spin-1/2 Heisenberg antiferromagnet on the triangular lattice might be a gapped spin-liquid state which is described by the $q = 2$ Laughlin state of bosons (22). That this model is classically frustrated motivates a description in terms of a quantum spin liquid. They investigated this phase of matter using variational studies. Taking N bosons at sites $\{\boldsymbol{r}_1, \boldsymbol{r}_2, \ldots \boldsymbol{r}_N\}$, the spin wave function considered is

$$|\Psi_{\text{KL}}\rangle \propto \sum_{\{\boldsymbol{r}_1, \boldsymbol{r}_2, \ldots, \boldsymbol{r}_N\}} \Psi^{\text{L}}_{q=2}(\boldsymbol{r}_1, \boldsymbol{r}_2, \ldots, \boldsymbol{r}_N) \prod_{n=1}^{N} b^\dagger_{\boldsymbol{r}_n} |\text{vac}\rangle \tag{30}$$

where $\Psi^{\text{L}}_{q=2}$ is the Laughlin wavefunction (22) with $z_i = (x_i + \mathrm{i}y_i)/\ell$ and $|\text{vac}\rangle = |\downarrow\rangle_1 \otimes |\downarrow\rangle_2 \ldots |\downarrow\rangle_N$. The wavefunction satisfies the hardcore constraint since $\Psi^{\text{L}}_2(\{\boldsymbol{r}_i\})$ vanishes when any two of its arguments coincide. Choosing N to be one half of the total number of sites of the triangular lattice, corresponding to a state with vanishing total spin component $S^z = 0$, and $4\pi\ell^2 = \sqrt{3}a_0^2$ (with a_0 the nearest neighbor spacing), Kalmeyer and Laughlin determined the variational energy of this state for the Heisenberg Hamiltonian, Eq. (29), and found it to be within 10% of other competing states. They argued for adiabatic continuity between this fractional quantum Hall wavefunction and the true ground state of the Heisenberg antiferromagnet. However, subsequent studies have shown that the ground state of this model is qualitatively distinct: it is magnetically ordered,[108,109] with correlations similar to those of the ground state of the classical antiferromagnet on this lattice.

Nevertheless, the Kalmeyer–Laughlin state remains a viable quantum spin-liquid phase which may appear in other models. Indeed, numerical studies of a frustrated Heisenberg model on the Kagomé lattice, with third-neighbor coupling, show evidence that the ground state spontaneously breaks time-reversal symmetry. It behaves as a gapped chiral spin liquid[110] with qualitative features of topological order (ground state degeneracy on a torus, and entanglement spectrum) that match those of the Kalmeyer–Laughlin state.[4] Such a phase has also been identified, through similar characteristics, for a Kagomé lattice model derived from the low energy limit of the Hubbard model in the presence of an orbital magnetic flux.[111] This flux explicitly breaks time-reversal symmetry and leads to the appearance of a chiral three-spin interaction that stabilizes the Kalmeyer–Laughlin phase.

Certain quantum magnets have been found to exhibit plateaus in the magnetization S_z as a function of external applied field B_z. In the boson picture, this corresponds to the mean boson density having plateaus as a function of chemical potential, i.e. incompressibility. Treating the bosons within a mean field Chern–Simons description, of the same form as the composite fermion construction described above

on the Harper–Hofstadter model, has been shown to reproduce the observed magnetization plateaus of the spin-1/2 antiferromagnetic on the Sutherland–Shastry[112] and Kagomé[113] lattices.

These examples draw close connections between standard FQH states of bosons and possible ground states of spin-1/2 quantum magnets. However they constitute a subset of a much broader class of quantum spin liquids[114] that is conceptually linked to fractional quantum Hall states. The deeper connections arise from the existence of topological order and associated fractionalized quasi-particles with anyonic statistics. A notable example is provided by the Kitaev honeycomb model,[115] describing a spin-1/2 lattice model in which the interactions between nearest neighbors are of XX, YY or ZZ type depending on the direction of the bond. This model is exactly solvable in terms of free Majorana fermions. In the presence of a magnetic field, which opens a gap it behaves as a chiral spin liquid with non-Abelian anyons. Recent studies of α-Ru-Cl$_3$ show the appearance of a plateau of the thermal Hall conductivity which is consistent with thermal transport by a Majorana edge mode.[116,117]

3.2. *Engineered qubit arrays*

There are now many experimental systems consisting of arrays of engineered two-level quantum systems which provide a class of many-body systems that are equivalent to spin-1/2 quantum magnets. The only difference from Sec. 3.1 is that the two-level quantum systems are designed and artificially constructed rather than provided by nature.

Atom or molecule arrays. Atoms or molecules subjected to deep optical lattices or strong optical tweezers can be formed into ordered arrays in which the positional degrees of freedom are frozen out. The internal excitations of these frozen atoms/molecules can provide a set of "spin" degrees of freedom. (These involve electronic/spin excitations for atoms and also ro-vibrational excitations for molecules.) The resulting two-level quantum systems can have very large coherence times, and can be coupled by dipolar interactions with timescales large compared to intrinsic decoherence times (e.g. from spontaneous emission). Experiments have shown coherent dynamics of coupled two-level systems, and evidence of strong (hardcore) interactions.[118,119] Theoretical proposals have shown how artificial magnetic fields can be imprinted for the motion of spins in two-dimensional arrays, leading to the possibility of forming FQH states: for rotational states of polar molecules[120] and for internal states of atoms in highly excited "Rydberg" states.[121]

Superconducting qubits. Circuit QED devices, based on superconducting structures, provide one of the leading approaches to generating engineered arrays of two-level quantum systems.[122] The two-level systems have splittings in the microwave frequency regime, so have negligible spontaneous emission, and are

readily controlled and coupled by resonant superconducting circuits. An experimental demonstration has been given of the basic elements required to break time-reversal symmetry and to imprint Peierls phase factors on the coupling between the qubits in a single three-site plaquette.[123] This follows the same approach as used in cold atoms,[34,36] described in Sec. 2.1.3, based on site-to-site detuning and re-establishing tunnelling by photon-assisted tunnelling through which Peierls phase factors can be imprinted. It has also been shown theoretically how time-reversal symmetry can be broken in such settings by coupling the qubits by resonator junctions made of passive elements subjected to static electric and magnetic fields.[124] A related, passive, scheme has been proposed based on the use of MW cavities with embedded magnetic materials. Such a MW resonator, designed to be described by the $n_\phi = 1/4$ Harper–Hofstadter model, has been constructed and the (topological) energy bands for photons measured.[125]

Topological Optical Resonators. Approaches similar to those of circuit QED have been pursued for two-level systems that operate in the optical domain. Much progress has been made in understanding how Chern bands can be generated for photonic structures operating in the optical frequency domain,[126] and there has been recent progress in various experimental settings.[107,127,128] Typically, such systems preserve time-reversal symmetry, for example, providing bands with opposite Chern numbers for the two polarizations of the light field. They also typically operate in regimes where interactions between photons are weak. However, strong interactions could, in principle, be introduced, for example, by embedding two-level atoms.[129]

3.3. *Continuum polaritons*

One way to ensure that there are strong interactions between photons is to embed them in a medium in which there is strong coupling such that the appropriate excitation is a polariton: an excitation that has both photon and matter components. Such polaritons can be formed in electronic materials, in which the matter component is an exciton, or in cold atomic gases, in which the matter component is an electronic excitation. The matter components of these polaritons can interact strongly. In both cases, the formation of a coherent polaritonic quasi-particle with long lifetime requires the photon to be held in an optical cavity, reducing its rate of loss.

Analogous to the effect of rotation on an atomic gas, one can engineer an artificial magnetic field for polaritons by rotating the medium through which the light is propagating.[130] This leads to a Landau level spectrum, as in Sec. 2.1.1, and has been shown to allow the formation of a Laughlin state of the polaritons. By coupling to highly-lying "Rydberg" levels of the atoms, the interactions can be made to be very strong and of tunable blockade radius, leading to models that show competing crystalline phases.[55]

Another way in which one can impose rotation on the polariton is to keep the medium stationary and to cause the optical field to rotate, by the use of a cavity that has a twisted character, such that repeated round-trip passage of rays of light within the cavity cause a rotation of the point of intersection of the ray with the medium. This can also be usefully viewed within a Floquet framework, the periodicity set by the time interval between successive transits of the central plane of the cavity.[131] The formation of Landau levels for the cavity modes has been demonstrated in experiment.[132] Theory has shown that, in the presence of a medium in which the light forms polaritons, the associated strong interactions provide ways to prepare the Laughlin state, and to allow measurements of exchange statistics.[133]

4. Concluding Remarks

We have summarized a range of physical settings in which one expects there to appear fractional quantum Hall states of bosons. Although no such state has yet been realized in experiment, this may soon change given the rapid technical advances in the relevant research areas. For bosons within continuum Landau levels, a key result is that the Laughlin state is the exact ground state for the naturally occurring form of two-body contact interactions. Numerical studies indicate stable and robust Moore–Read and Read–Rezayi states, offering the prospect that these systems may allow experimental investigation of non-Abelian phases.

Many of the proposed physical realizations bring in physics that is uncommon in electronic systems. Cold atomic gases could allow for the study of the interplay of strong-pairing superconductivity and FQH physics. Achieving FQH states at high particle density in cold gases naturally leads to lattice-based models, and can allow for novel FQH states that exist only on lattices, notably in bands with Chern number $|\mathcal{C}| > 1$. FQH states of optical photons/polaritons typically involve particle loss, so operation requires pumping and dissipation,[134,135] also bringing novel features compared to the equilibrium situations typically considered for electronic materials.

Theoretical analyses have identified many novel experimental settings in which FQH states of bosons could appear. These theories have been guided by the existing understanding of FQH systems, which has been built on experimental discoveries in electronic systems. It is clear that much remains to be understood about strongly interacting quantum many body systems. The new physical settings for bosonic matter are sufficiently different from electronic systems that existing theories may be inadequate to understand all of their features, and the experimental explorations have the scope to uncover qualitatively new phenomena that were previously unexpected.

Acknowledgments

stimulating interactions. I also gratefully acknowledge research support by EPSRC grant EP/P034616/1 and by a Simons Investigator Award.

References

1. D. C. Tsui, H. L. Stormer, and A. C. Gossard, Two-dimensional magnetotransport in the extreme quantum limit, *Phys. Rev. Lett.* **48**, 1559–1562 (1982).
2. E. M. Spanton, A. A. Zibrov, H. Zhou, T. Taniguchi, K. Watanabe, M. P. Zaletel, and A. F. Young, Observation of fractional Chern insulators in a van der Waals heterostructure, *Science.* **360**(6384), 62–66 (2018).
3. R. B. Laughlin, Anomalous quantum Hall effect: An incompressible quantum fluid with fractionally charged excitations, *Phys. Rev. Lett.* **50**, 1395–1398 (1983).
4. V. Kalmeyer and R. B. Laughlin, Equivalence of the resonating-valence-bond and fractional quantum Hall states, *Phys. Rev. Lett.* **59**, 2095–2098 (1987).
5. I. Bloch, J. Dalibard, and W. Zwerger, Many-body physics with ultracold gases, *Rev. Mod. Phys.* **80**, 885–964 (2008).
6. C. J. Pethick and H. Smith, *Bose–Einstein Condensation in Dilute Gases.* (Cambridge University Press, 2008).
7. M. Olshanii, Atomic scattering in the presence of an external confinement and a gas of impenetrable bosons, *Phys. Rev. Lett.* **81**, 938–941 (1998).
8. M. A. Baranov, M. Dalmonte, G. Pupillo, and P. Zoller, Condensed matter theory of dipolar quantum gases, *Chem. Rev.* **112**(9), 5012–5061 (2012).
9. A. L. Fetter, Rotating trapped Bose–Einstein condensates, *Rev. Mod. Phys.* **81**, 647–691 (2009).
10. N. R. Cooper, Rapidly rotating atomic gases, *Adv. Phys.* **57**(6), 539–616 (2008).
11. N. R. Cooper, J. Dalibard, and I. B. Spielman, Topological bands for ultracold atoms, *Rev. Mod. Phys.* **91**(1), 015005 (2019).
12. L. D. Landau and E. M. Lifshitz, *Statistical Physics Pt 1.* Vol. 5, (Butterworth Heinemann, Oxford, 1981).
13. N. K. Wilkin, J. M. F. Gunn, and R. A. Smith, Do attractive bosons condense?, *Phys. Rev. Lett.* **80**, 2265–2268 (1998).
14. V. Schweikhard, I. Coddington, P. Engels, S. Tung, and E. A. Cornell, Vortex-lattice dynamics in rotating spinor Bose–Einstein condensates, *Phys. Rev. Lett.* **93**(21), 210403 (2004).
15. N. Gemelke, E. Sarajlic, and S. Chu, Rotating few-body atomic systems in the fractional quantum Hall regime, *arXiv e-prints.* art. arXiv:1007.2677 (2010).
16. S. Kuhr, Quantum-gas microscopes: A new tool for cold-atom quantum simulators, *Nat. Sci. Rev.* **3**(2), 170–172 (2016).
17. C. Cohen-Tannoudji, J. Dupont-Roc, and G. Grynberg, *Atom-Photon Interactions.* (Wiley, New York, 1992).
18. Y.-J. Lin, R. L. Compton, A. R. Perry, W. D. Phillips, J. V. Porto, and I. B. Spielman, Bose–Einstein condensate in a uniform light-induced vector potential, *Phys. Rev. Lett.* **102**(13):130401 (2009).
19. N. R. Cooper, Optical flux lattices for ultracold atomic gases, *Phys. Rev. Lett.* **106**(17), 175301 (2011).
20. D. J. Thouless, M. Kohmoto, M. P. Nightingale, and M. den Nijs, Quantized Hall conductance in a two-dimensional periodic potential, *Phys. Rev. Lett.* **49**(6), 405–408 (1982).

21. N. R. Cooper and R. Moessner, Designing topological bands in reciprocal space, *Phys. Rev. Lett.* **109**, 215302 (2012).

22. Y.-L. Wu, N. Regnault, and B. A. Bernevig, Bloch model wave functions and pseudopotentials for all fractional Chern insulators, *Phys. Rev. Lett.* **110**, 106802 (2013).

23. N. R. Cooper and J. Dalibard, Optical flux lattices for two-photon dressed states, *Europhys. Lett.* **95**(6), 66004 (2011).

24. N. R. Cooper and J. Dalibard, Reaching fractional quantum Hall states with optical flux lattices, *Phys. Rev. Lett.* **110**, 185301 (2013).

25. D. Jaksch and P. Zoller, Creation of effective magnetic fields in optical lattices: The Hofstadter butterfly for cold neutral atoms, *New J. Phys.* **5**, 56 (2003).

26. F. Gerbier and J. Dalibard, Gauge fields for ultracold atoms in optical superlattices, *New J. Phys.* **12**(3), 033007 (2010).

27. W. Sun, B.-Z. Wang, X.-T. Xu, C.-R. Yi, L. Zhang, Z. Wu, Y. Deng, X.-J. Liu, S. Chen, and J.-W. Pan, Highly controllable and robust 2d spin-orbit coupling for quantum gases, *Phys. Rev. Lett.* **121**, 150401 (2018).

28. A. Eckardt, Atomic quantum gases in periodically driven optical lattices, *Rev. Mod. Phys.* **89**, 011004 (2017).

29. G. Jotzu, M. Messer, R. Desbuquois, M. Lebrat, T. Uehlinger, D. Greif, and T. Esslinger, Experimental realization of the topological Haldane model with ultracold fermions, *Nature.* **515**(7526), 237–240 (2014).

30. T. Oka and H. Aoki, Photovoltaic Hall effect in graphene, *Phys. Rev. B.* **79**, 081406 (2009).

31. F. D. M. Haldane, Model for a quantum Hall effect without Landau levels: Condensed-matter realization of the "parity anomaly", *Phys. Rev. Lett.* **61**(18), 2015–2018 (1988).

32. P. G. Harper, The general motion of conduction electrons in a uniform magnetic field, with application to the diamagnetism of metals, *Proc. Phys. Soc. A.* **68**(10), 879 (1955).

33. D. R. Hofstadter, Energy levels and wave functions of Bloch electrons in rational and irrational magnetic fields, *Phys. Rev. B.* **14**(6), 2239–2249 (1976).

34. M. Aidelsburger, M. Atala, M. Lohse, J. T. Barreiro, B. Paredes, and I. Bloch, Realization of the Hofstadter Hamiltonian with ultracold atoms in optical lattices, *Phys. Rev. Lett.* **111**, 185301 (2013).

35. M. Aidelsburger, M. Lohse, C. Schweizer, M. Atala, J. T. Barreiro, S. Nascimbène, N. R. Cooper, I. Bloch, and N. Goldman, Measuring the Chern number of Hofstadter bands with ultracold bosonic atoms, *Nat. Phys.* **111**, 162–166 (2015).

36. H. Miyake, G. A. Siviloglou, C. J. Kennedy, W. C. Burton, and W. Ketterle, Realizing the Harper Hamiltonian with laser-assisted tunneling in optical lattices, *Phys. Rev. Lett.* **111**, 185302 (2013).

37. M. E. Tai, A. Lukin, M. Rispoli, R. Schittko, T. Menke, D. Borgnia, P. M. Preiss, F. Grusdt, A. M. Kaufman, and M. Greiner, Microscopy of the interacting Harper–Hofstadter model in the two-body limit, *Nature.* **546**, 519–523 (2017).

38. F. D. M. Haldane, Fractional quantization of the Hall effect: A hierarchy of incompressible quantum fluid states, *Phys. Rev. Lett.* **51**, 605–608 (1983).

39. N. R. Cooper, S. Komineas, and N. Read, Vortex lattices in the lowest Landau level for confined Bose–Einstein condensates, *Phys. Rev. A.* **70**, 033604 (2004).

40. G. Baym, Vortex lattices in rapidly rotating Bose–Einstein condensates: Modes and correlation functions, *Phys. Rev. A.* **69**, 043618 (2004).

41. S. Moroz, C. Hoyos, C. Benzoni, and D. T. Son, Effective field theory of a vortex lattice in a bosonic superfluid, *SciPost Phys.* **5**, 39 (2018).

42. N. R. Cooper, N. K. Wilkin, and J. M. F. Gunn, Quantum phases of vortices in rotating Bose–Einstein condensates, *Phys. Rev. Lett.* **87**, 120405 (2001).

43. E. H. Lieb, R. Seiringer, and J. Yngvason, Yrast line of a rapidly rotating Bose gas: Gross–Pitaevskii regime, *Phys. Rev. A.* **79**, 063626 (2009).

44. N. R. Cooper and E. H. Rezayi, Competing compressible and incompressible phases in rotating atomic Bose gases at filling factor $\nu = 2$, *Phys. Rev. A.* **75**, 013627 (2007).

45. N. R. Cooper and N. K. Wilkin, Composite fermion description of rotating Bose–Einstein condensates, *Phys. Rev. B.* **60**, R16279–R16282 (1999).

46. J. K. Jain, *Composite fermions*. (Cambridge University Press, 2007).

47. N. Regnault and T. Jolicoeur, Quantum Hall fractions in rotating Bose–Einstein condensates, *Phys. Rev. Lett.* **91**, 030402 (2003).

48. B. I. Halperin, P. A. Lee, and N. Read, Theory of the half-filled Landau level, *Phys. Rev. B.* **47**, 7312–7343 (1993).

49. G. Moore and N. Read, Non-Abelions in the fractional quantum Hall effect, *Nucl. Phys. B.* **360**, 362–396 (1991).

50. N. Read and E. Rezayi, Beyond paired quantum Hall states: Parafermions and incompressible states in the first excited Landau level, *Phys. Rev. B.* **59**, 8084–8092 (1999).

51. A. Cappelli, L. S. Georgiev, and I. T. Todorov, Parafermion Hall states from coset projections of Abelian conformal theories, *Nucl. Phys. B.* **599**(3), 499–530 (2001).

52. C. Nayak, S. H. Simon, A. Stern, M. Freedman, and S. D. Sarma, Non-Abelian anyons and topological quantum computation, *Rev. Mod. Phys.* **80**(3):1083 (2008).

53. E. H. Rezayi, N. Read, and N. R. Cooper, Incompressible liquid state of rapidly rotating bosons at filling factor 3/2, *Phys. Rev. Lett.* **95**, 160404 (2005).

54. N. R. Cooper, E. H. Rezayi, and S. H. Simon, Vortex lattices in rotating atomic Bose gases with dipolar interactions, *Phys. Rev. Lett.* **95**, 200402 (2005).

55. F. Grusdt and M. Fleischhauer, Fractional quantum Hall physics with ultracold Rydberg gases in artificial gauge fields, *Phys. Rev. A.* **87**, 043628 (2013).

56. G. Möller and N. R. Cooper, Density waves and supersolidity in rapidly rotating atomic Fermi gases, *Phys. Rev. Lett.* **99**, 190409 (2007).

57. K. Yang and H. Zhai, Quantum Hall transition near a fermion Feshbach resonance in a rotating trap, *Phys. Rev. Lett.* **100**, 030404 (2008).

58. C. Repellin, T. Yefsah, and A. Sterdyniak, Creating a bosonic fractional quantum Hall state by pairing fermions, *Phys. Rev. B.* **96**, 161111 (2017).

59. Z. Tešanović, F. M. C. Axel, and B. I. Halperin, "Hall crystal" versus Wigner crystal, *Phys. Rev. B.* **39**, 8525–8551 (1989).

60. A. Kol and N. Read, Fractional quantum Hall effect in a periodic potential, *Phys. Rev. B.* **48**, 8890–8898 (1993).

61. S. A. Parameswaran, R. Roy, and S. L. Sondhi, Fractional quantum Hall physics in topological flat bands, *Comptes Rendus Physique.* **14**(9), 816–839 (2013).

62. E. J. Bergholtz and Z. Liu, Toplogical flat band models and fractional Chern insulators, *Int. J. Mod. Phys. B.* **27**(24), 1330017 (2013).

63. T. Neupert, C. Chamon, T. Iadecola, L. H. Santos, and C. Mudry, Fractional (Chern and topological) insulators, *Physica Scripta.* **T164**, 014005 (2015).

64. A. S. Sørensen, E. Demler, and M. D. Lukin, Fractional quantum Hall states of atoms in optical lattices, *Phys. Rev. Lett.* **94**(8):086803 (2005).

65. M. Hafezi, A. S. Sørensen, E. Demler, and M. D. Lukin, Fractional quantum Hall effect in optical lattices, *Phys. Rev. A.* **76**(2):023613 (2007).

66. G. Möller and N. R. Cooper, Composite fermion theory for bosonic quantum Hall states on lattices, *Phys. Rev. Lett.* **103**, 105303 (2009).

67. Y.-C. He, F. Grusdt, A. Kaufman, M. Greiner, and A. Vishwanath, Realizing and adiabatically preparing bosonic integer and fractional quantum Hall states in optical lattices, *Phys. Rev. B.* **96**, 201103 (2017).

68. D. Bauer, T. S. Jackson, and R. Roy, Quantum geometry and stability of the fractional quantum Hall effect in the Hofstadter model, *Phys. Rev. B.* **93**, 235133 (2016).

69. A. Sterdyniak, B. A. Bernevig, N. R. Cooper, and N. Regnault, Interacting bosons in topological optical flux lattices, *Phys. Rev. B.* **91**, 035115 (2015).

70. E. Kapit and E. Mueller, Exact parent Hamiltonian for the quantum Hall states in a lattice, *Phys. Rev. Lett.* **105**, 215303 (2010).

71. I. Glasser, J. I. Cirac, G. Sierra, and A. E. B. Nielsen, Lattice effects on Laughlin wave functions and parent Hamiltonians, *Phys. Rev. B.* **94**, 245104 (2016).

72. G. Möller and N. R. Cooper, Fractional Chern insulators in Harper–Hofstadter bands with higher Chern number, *Phys. Rev. Lett.* **115**, 126401 (2015).

73. G. H. Wannier, A result not dependent on rationality for Bloch electrons in a magnetic field, *Physica Status Solidi B.* **88**(2), 757–765 (1978).

74. P. Středa, Quantised Hall effect in a two-dimensional periodic potential, *J. Phys. C: Solid State Physics.* **15**(36), L1299–L1303 (1982).

75. T. Senthil, Symmetry-protected topological phases of quantum matter, *Ann. Rev. Conden. Matt. Phys.* **6**(1), 299–324 (2015).

76. T. Senthil and M. Levin, Integer quantum Hall effect for bosons, *Phys. Rev. Lett.* **110**, 046801 (2013).

77. A. Sterdyniak, N. R. Cooper, and N. Regnault, Bosonic integer quantum Hall effect in optical flux lattices, *Phys. Rev. Lett.* **115**, 116802 (2015).

78. B. I. Halperin, Theory of the quantized Hall resistance, *Helv. Phys. Acta.* **56**, 75 (1983).

79. M. Barkeshli and X.-L. Qi, Topological nematic states and non-Abelian lattice dislocations, *Phys. Rev. X.* **2**, 031013 (2012).

80. M. J. H. Ku, A. T. Sommer, L. W. Cheuk, and M. W. Zwierlein, Revealing the superfluid lambda transition in the universal thermodynamics of a unitary Fermi gas, *Science.* **335**(6068), 563–567 (2012).

81. N. R. Cooper, F. J. M. van Lankvelt, J. W. Reijnders, and K. Schoutens, Quantum Hall states of atomic Bose gases: Density profiles in single-layer and multilayer geometries, *Phys. Rev. A.* **72**, 063622 (2005).

82. N. Read and N. R. Cooper, Free expansion of lowest-Landau-level states of trapped atoms: A wave-function microscope, *Phys. Rev. A.* **68**, 035601 (2003).

83. D. Husmann, M. Lebrat, S. Häusler, J.-P. Brantut, L. Corman, and T. Esslinger, Breakdown of the Wiedemann–Franz law in a unitary Fermi gas, *Proc. Nat. Acad. Sci.* **115**(34), 8563–8568 (2018).

84. M. Aidelsburger, M. Lohse, C. Schweizer, M. Atala, J. T. Barreiro, S. Nascimbène, N. R. Cooper, I. Bloch, and N. Goldman, Measuring the Chern number of Hofstadter bands with ultracold bosonic atoms, *Nat. Phys.* **11**, 162 (2015).

85. D. T. Tran, A. Dauphin, A. G. Grushin, P. Zoller, and N. Goldman, Probing topology by 'heating': Quantized circular dichroism in ultracold atoms, *Sci. Adv.* **3**(8), e1701207 (2017).

86. L. Asteria, D. T. Tran, T. Ozawa, M. Tarnowski, B. S. Rem, N. Fläschner, K. Sengstock, N. Goldman, and C. Weitenberg, Measuring quantized circular dichroism in ultracold topological matter, *Nat. Phys.* **15**, 449 (2019).

87. J. Stenger, S. Inouye, A. P. Chikkatur, D. M. Stamper-Kurn, D. E. Pritchard, and W. Ketterle, Bragg spectroscopy of a Bose–Einstein condensate, *Phys. Rev. Lett.* **82**, 4569–4573 (1999).

88. J. Steinhauer, R. Ozeri, N. Katz, and N. Davidson, Excitation spectrum of a Bose–Einstein condensate, *Phys. Rev. Lett.* **88**, 120407 (2002).

89. S. Hoinka, M. Lingham, K. Fenech, H. Hu, C. J. Vale, J. E. Drut, and S. Gandolfi, Precise determination of the structure factor and contact in a unitary Fermi gas, *Phys. Rev. Lett.* **110**, 055305 (2013).

90. S. Stringari, Collective excitations of a trapped Bose-condensed gas, *Phys. Rev. Lett.* **77**, 2360–2363 (1996).

91. M. A. Cazalilla, N. Barberán, and N. R. Cooper, Edge excitations and topological order in a rotating Bose gas, *Phys. Rev. B.* **71**, 121303 (2005).

92. N. R. Cooper and S. H. Simon, Signatures of fractional exclusion statistics in the spectroscopy of quantum Hall droplets, *Phys. Rev. Lett.* **114**, 106802 (2015).

93. B. Paredes, P. Fedichev, J. I. Cirac, and P. Zoller, 1/2-anyons in small atomic Bose–Einstein condensates, *Phys. Rev. Lett.* **87**, 010402 (2001).

94. E. Kapit, P. Ginsparg, and E. Mueller, Non-Abelian braiding of lattice bosons, *Phys. Rev. Lett.* **108**, 066802 (2012).

95. Y. Zhang, G. J. Sreejith, N. D. Gemelke, and J. K. Jain, Fractional angular momentum in cold-atom systems, *Phys. Rev. Lett.* **113**, 160404 (2014).

96. Y. Zhang, G. J. Sreejith, and J. K. Jain, Creating and manipulating non-Abelian anyons in cold atom systems using auxiliary bosons, *Phys. Rev. B.* **92**, 075116 (2015).

97. D. Lundholm and N. Rougerie, Emergence of fractional statistics for tracer particles in a Laughlin liquid, *Phys. Rev. Lett.* **116**, 170401 (2016).

98. F. Grusdt, N. Y. Yao, D. Abanin, M. Fleischhauer, and E. Demler, Interferometric measurements of many-body topological invariants using mobile impurities, *Nat. Commun.* **7**, 11994 (2016).

99. S. K. Baur, K. R. A. Hazzard, and E. J. Mueller, Stirring trapped atoms into fractional quantum Hall puddles, *Phys. Rev. A.* **78**, 061608 (2008).

100. J. Motruk and F. Pollmann, Phase transitions and adiabatic preparation of a fractional Chern insulator in a boson cold-atom model, *Phys. Rev. B.* **96**, 165107 (2017).

101. M. Popp, B. Paredes, and J. I. Cirac, Adiabatic path to fractional quantum Hall states of a few bosonic atoms, *Phys. Rev. A.* **70**, 053612 (2004).

102. J. Zhang, J. Beugnon, and S. Nascimbene, Creating fractional quantum Hall states with atomic clusters using light-assisted insertion of angular momentum, *Phys. Rev. A.* **94**, 043610 (2016).

103. F. Grusdt, F. Letscher, M. Hafezi, and M. Fleischhauer, Topological growing of Laughlin states in synthetic gauge fields, *Phys. Rev. Lett.* **113**, 155301 (2014).

104. M. Roncaglia, M. Rizzi, and J. I. Cirac, Pfaffian state generation by strong three-body dissipation, *Phys. Rev. Lett.* **104**, 096803 (2010).

105. M. Greiner, O. Mandel, T. Esslinger, T. W. Hänsch, and I. Bloch, Quantum phase transition from a superfluid to a mott insulator in a gas of ultracold atoms, *Nature.* **415**(6867), 39 (2002).

106. M. Aidelsburger, S. Nascimbene, and N. Goldman, Artificial gauge fields in materials and engineered systems, *Comptes Rendus Physique.* **19**(6), 394–432 (2018).

107. T. Ozawa, H. M. Price, A. Amo, N. Goldman, M. Hafezi, L. Lu, M. C. Rechtsman, D. Schuster, J. Simon, O. Zilberberg, and I. Carusotto, Topological photonics, *Rev. Mod. Phys.* **91**, 015006 (2019).

108. L. Capriotti, A. E. Trumper, and S. Sorella, Long-range Néel order in the triangular Heisenberg model, *Phys. Rev. Lett.* **82**, 3899–3902 (1999).

109. S. R. White and A. L. Chernyshev, Néel order in square and triangular lattice Heisenberg models, *Phys. Rev. Lett.* **99**, 127004 (2007).

110. Y.-C. He, D. N. Sheng, and Y. Chen, Chiral spin liquid in a frustrated anisotropic Kagome Heisenberg model, *Phys. Rev. Lett.* **112**, 137202 (2014).

111. B. Bauer, L. Cincio, B. P. Keller, M. Dolfi, G. Vidal, S. Trebst, and A. W. W. Ludwig, Chiral spin liquid and emergent anyons in a Kagome lattice Mott insulator, *Nat. Commun.* **5**, 5137 (2014).

112. G. Misguich, T. Jolicoeur, and S. M. Girvin, Magnetization plateaus of $SrCu_2(BO_3)_2$ from a Chern–Simons theory, *Phys. Rev. Lett.* **87**, 097203 (2001).

113. K. Kumar, K. Sun, and E. Fradkin, Chern–Simons theory of magnetization plateaus of the spin-$\frac{1}{2}$ quantum XXZ Heisenberg model on the Kagome lattice, *Phys. Rev. B.* **90**, 174409 (2014).

114. L. Savary and L. Balents, Quantum spin liquids: A review, *Rep. Prog. Phys.* **80**(1), 016502 (2017).

115. A. Kitaev, Anyons in an exactly solved model and beyond, *Ann. Phys.* **321**(1), 2–111 (2006).

116. Y. Kasahara, K. Sugii, T. Ohnishi, M. Shimozawa, M. Yamashita, N. Kurita, H. Tanaka, J. Nasu, Y. Motome, T. Shibauchi, and Y. Matsuda, Unusual thermal Hall effect in a Kitaev spin liquid candidate α-$RuCl_3$, *Phys. Rev. Lett.* **120**, 217205 (2018).

117. Y. Kasahara, T. Ohnishi, Y. Mizukami, O. Tanaka, S. Ma, K. Sugii, N. Kurita, H. Tanaka, J. Nasu, Y. Motome, T. Shibauchi, and Y. Matsuda, Majorana quantization and half-integer thermal quantum Hall effect in a Kitaev spin liquid, *Nature.* **559**(7713), 227–231 (2018).

118. H. Levine, A. Keesling, A. Omran, H. Bernien, S. Schwartz, A. S. Zibrov, M. Endres, M. Greiner, V. Vuletić, and M. D. Lukin, High-fidelity control and entanglement of Rydberg-atom qubits, *Phys. Rev. Lett.* **121**, 123603 (2018).

119. S. de Léséleuc, V. Lienhard, P. Scholl, D. Barredo, S. Weber, N. Lang, H. P. Büchler, T. Lahaye, and A. Browaeys, Observation of a symmetry-protected topological phase of interacting bosons with Rydberg atoms, *Science* **365**, 775 (2019).

120. N. Y. Yao, A. V. Gorshkov, C. R. Laumann, A. M. Läuchli, J. Ye, and M. D. Lukin, Realizing fractional Chern insulators in dipolar spin systems, *Phys. Rev. Lett.* **110**, 185302 (2013).

121. M. F. Maghrebi, N. Y. Yao, M. Hafezi, T. Pohl, O. Firstenberg, and A. V. Gorshkov, Fractional quantum Hall states of Rydberg polaritons, *Phys. Rev. A.* **91**, 033838 (2015).

122. S. Schmidt and J. Koch, Circuit QED lattices: Towards quantum simulation with superconducting circuits, *Annalen der Physik.* **525**(6), 395–412 (2013).

123. P. Roushan, C. Neill, A. Megrant, Y. Chen, R. Babbush, R. Barends, B. Campbell, Z. Chen, B. Chiaro, A. Dunsworth, A. Fowler, E. Jeffrey, J. Kelly, E. Lucero, J. Mutus, P. J. J. O'Malley, M. Neeley, C. Quintana, D. Sank, A. Vainsencher, J. Wenner, T. White, E. Kapit, H. Neven, and J. Martinis, Chiral ground-state currents of interacting photons in a synthetic magnetic field, *Nat. Phys.* **13**, 146 (2016).

124. J. Koch, A. A. Houck, K. L. Hur, and S. M. Girvin, Time-reversal-symmetry breaking in circuit-QED-based photon lattices, *Phys. Rev. A.* **82**, 043811 (2010).

125. C. Owens, A. LaChapelle, B. Saxberg, B. M. Anderson, R. Ma, J. Simon, and D. I. Schuster, Quarter-flux Hofstadter lattice in a qubit-compatible microwave cavity array, *Phys. Rev. A.* **97**(1), 013818 (2018).

126. S. Raghu and F. D. M. Haldane, Analogs of quantum-Hall-effect edge states in photonic crystals, *Phys. Rev. A.* **78**, 033834 (2008).

127. L. Lu, J. D. Joannopoulos, and M. Soljačić, Topological photonics, *Nat. Phot.* **8**, 821 (2014).

128. S. Mittal, S. Ganeshan, J. Fan, A. Vaezi, and M. Hafezi, Measurement of topological invariants in a 2D photonic system, *Nat. Phot.* **10**, 180 (2016).

129. J. Cho, D. G. Angelakis, and S. Bose, Fractional quantum Hall state in coupled cavities, *Phys. Rev. Lett.* **101**, 246809 (2008).

130. J. Otterbach, J. Ruseckas, R. G. Unanyan, G. Juzeliūnas, and M. Fleischhauer, Effective magnetic fields for stationary light, *Phys. Rev. Lett.* **104**, 033903 (2010).

131. A. Sommer and J. Simon, Engineering photonic Floquet Hamiltonians through Fabry–Pérot resonators, *New J. Phys.* **18**(3), 035008 (2016).

132. N. Schine, A. Ryou, A. Gromov, A. Sommer, and J. Simon, Synthetic Landau levels for photons, *Nature.* **534**, 671 (2016).

133. S. Dutta and E. J. Mueller, Coherent generation of photonic fractional quantum Hall states in a cavity and the search for anyonic quasiparticles, *Phys. Rev. A.* **97**, 033825 (2018).

134. R. O. Umucalilar and I. Carusotto, Fractional quantum Hall states of photons in an array of dissipative coupled cavities, *Phys. Rev. Lett.* **108**, 206809 (2012).

135. I. Carusotto and C. Ciuti, Quantum fluids of light, *Rev. Mod. Phys.* **85**, 299–366 (2013).